We are IntechOpen, the world's leading publisher of Open Access books Built by scientists, for scientists

6,900
Open access books available

185,000
International authors and editors

200M
Downloads

Our authors are among the

154
Countries delivered to

TOP 1%
most cited scientists

12.2%
Contributors from top 500 universities



WEB OF SCIENCE™

Selection of our books indexed in the Book Citation Index in Web of Science™ Core Collection (BKCI)

Interested in publishing with us?
Contact book.department@intechopen.com

Numbers displayed above are based on latest data collected.
For more information visit www.intechopen.com



Chapter 9

Preparation and Self-assembly of Functionalized Nanocomposites and Nanomaterials – Relationship Between Structures and Properties

Tifeng Jiao, Jie Hu, Qingrui Zhang and Yong Xiao

Additional information is available at the end of the chapter

http://dx.doi.org/10.5772/60796

Abstract

The recent progress in nanocomposites and nanomaterials is varied and occupies various fields. Nanocomposites can be prepared with a variety of special physical, thermal, and other unique properties. On the other hand, self-assembly technique is playing an important role in preparing well-defined multilevel nanostructures and the functionalized surface with the designed and controlled properties. In this chapter, various kinds of nanocomposites including gold nanoparticles, inorganic-organic hybrid composites, graphene oxide nanocomposites, and supramolecular gels via functionalized imide amphiphiles/binary mixtures have all been investigated and analyzed. We summarize main research contributions in recent years in three sections: preparation and self-assembly of some functionalized hybrid nanostructures; preparation and self-assembly of some graphene oxide nanocomposites; preparation and self-assembly of supramolecular gels based on some functionalized imide amphiphiles/binary mixtures. The above work may give the potential perspective for the design and fabrication of nanomaterials and composites. New nanocomposites and nanomaterials are emerging as sensitive study platforms based on unique optical and electrical properties. Future research on preparation of nanocomposites and nanomaterials will depend on the less-expensive processes in order to produce low-cost nanomaterials and devices.

Keywords: nanocomposites, nanomaterials, self-assembly, nanostructures, properties

INTECH
open science | open minds

© 2015 The Author(s). Licensee InTech. This chapter is distributed under the terms of the Creative Commons Attribution License (http://creativecommons.org/licenses/by/3.0), which permits unrestricted use, distribution, and reproduction in any medium, provided the original work is properly cited.

1. Introduction

The recent progress in nanocomposites and nanomaterials is varied and occupies various fields [1–5]. Nanocomposites can be prepared with a variety of special physical, thermal, and other unique properties. They have better properties than conventional microscale composites and can be synthesized using simple and inexpensive techniques. Now, in a broad sense the word "composite" means "made of two or more different parts" or "a composite is a combination of two or more different materials that are mixed in an effort to blend the best properties of both". A composite material consists of an assemblage of two materials of different natures completing and allowing us to obtain a material of which the set of performance characteristics is greater than that of the components taken separately. Mostly, composite material consists of one or more discontinuous phases distributed in one continuous phase. Hybrid components are that which are with several discontinuous phases of different natures. Discontinuous phase is usually harder and with superior mechanical properties than continuous phase. Nanomaterials and nanocomposites often have unique properties that could enable composite materials with multiple unique properties simultaneously; however, it is often challenging to achieve these properties in large-scale nanocomposite materials. Furthermore, it is important that nanomaterials have desirable properties that cannot be achieved through use of conventional chemicals and materials. To assess the potential value of nanocomposites, it is important to determine which nanomaterials can be effectively integrated into nanocomposites and what new or improved properties are enabled by this. Thus, models of the interactions within the nanocomposites are needed to enable development of effective rules of mixtures. This may require a combination of numerical modeling, characterization, and informatics to enable this nanocomposite with properties by design capability.

On the other hand, self-assembly technique is playing an important role in preparing well-defined multilevel nanostructures and the functionalized surface with the designed and controlled properties [6–8]. Unlike the conventional self-assemblies of amphiphilic compounds at various interfaces or in the bulk, the self-assembly process of the various nanoparticles, colloidal microspheres, metallo-supramolecular systems, inorganic-organic hybrids, and supramolecular nanostructures exhibits unusual advantages, especially in fabricating complicated nanomaterials and nanocomposites. The addition of nanocomposites to self-assembly has enabled new properties for the composite material, but results are highly dependent on the organized arrangement of the nanocomposites and the processing used. It is important to determine whether nanomaterials could be integrated into nanocomposites to enable multiple desirable properties required for a given application.

In our recent research, some functionalized nanocomposites and nanomaterials have been prepared and investigated. In addition, some of the analytical methods, theoretical treatments, and synthetic tools, which are being applied in the area of self-assembly and supramolecular chemistry, will be highlighted. In this chapter, we summarize our main research contributions in recent years in three sections: (1) preparation and self-assembly of some functionalized hybrid nanostructures; (2) preparation and self-assembly of some graphene oxide nanocomposites; (3) preparation and self-assembly of supramolecular gels based on some functionalized imide amphiphiles / binary mixtures.

http://dx.doi.org/10.5772/60796

2. Preparation and self-assembly of some functionalized hybrid nanostructures

In recent years, as a kind of important materials in nanoscience and nanotechnology, gold nanoparticles have been studied most [9–11]. As reported in previous literatures, many methods [12–14] and various kinds of capping agents [15–18] have been investigated to prepare functionalized gold nanoparticles with designed and tailored properties. The capacity to regulate size, shape, and surface functionalized groups to create certain surface properties as well as to manipulate the colloid stability of nanoparticle dispersions are important factors related to their practical applications [19–21]. On the other hand, since the self-assembled nanostructures are very sensitive to and dependent on the molecular skeletons in amphiphile compounds, the design and synthesis of amphiphilic molecules are of utmost importance. In this part, we have demonstrated some examples of such systems including preparation of gold nanoparticles by a series of amphiphiles with hydrophilic ethyleneamine spacers and aromatic headgroups at liquid–liquid interface. Interestingly, it was found that different gold nanostructures were obtained due to different substituted headgroups. The photocatalytic properties of as-made gold nanoparticles on the degradation of methyl orange were also investigated. At the same time, some amorphous nanocomposites were fabricated using chemical precipitation methods. All the results rendered us to believe that these nanocomposites are promising adsorbents for enhanced phosphate removal from contaminated waters.

Based on the research background, some gold nanoparticles were synthesized via a series of bolaform amphiphiles with hydrophilic ethyleneamine spacers and aromatic headgroups at a liquid–liquid interface [22]. By stirring the aqueous $AuCl_4^-$ ions solution with the chloroform solution of used Schiff base compounds, $AuCl_4^-$ ions were transferred into the chloroform phase and reduced to gold nanoparticles. Various gold nanoparticles and nanostructures have been gained depending on the different molecular skeletons and spacers, headgroups of bolaform Schiff base compounds, and the molar ratios of compounds to $AuCl_4^-$ ions. Morphological and spectral investigations suggested that used bolaform Schiff base compounds could act as both capping and reducing agents. For example, the selected-area electron diffraction (SAED) was done on a single nanostructure on a copper grid, as shown in Figure 1. From the SAED patterns, as for the gold nanostructures generated by NpN1 and NpN2 with amphiphile to chloroaurate ion ratio of 1:2, strong electron diffraction patterns were dominated, indicating the crystalline nature of these nanostructures. In addition, the photocatalytic properties of as-prepared gold nanoparticles on the degradation of dye (methyl orange as example) were investigated, demonstrating the effect of substituted groups and molecular skeletons in the compounds on the sizes of as-prepared gold nanoparticles and subsequent catalytic behaviors. The present research results indicated that gold nanostructures could be prepared and designed by bolaform Schiff base compounds and could be well regulated by changing various substituted skeletons and groups (headgroups and spacers).

In addition, some other gold nanoparticles were synthesized by two bolaform cholesteryl imide derivatives with different lengths of ethyleneamine spacers at a liquid–liquid interface [23]. Spectral and morphological measurements indicated that both bolaform amphiphiles

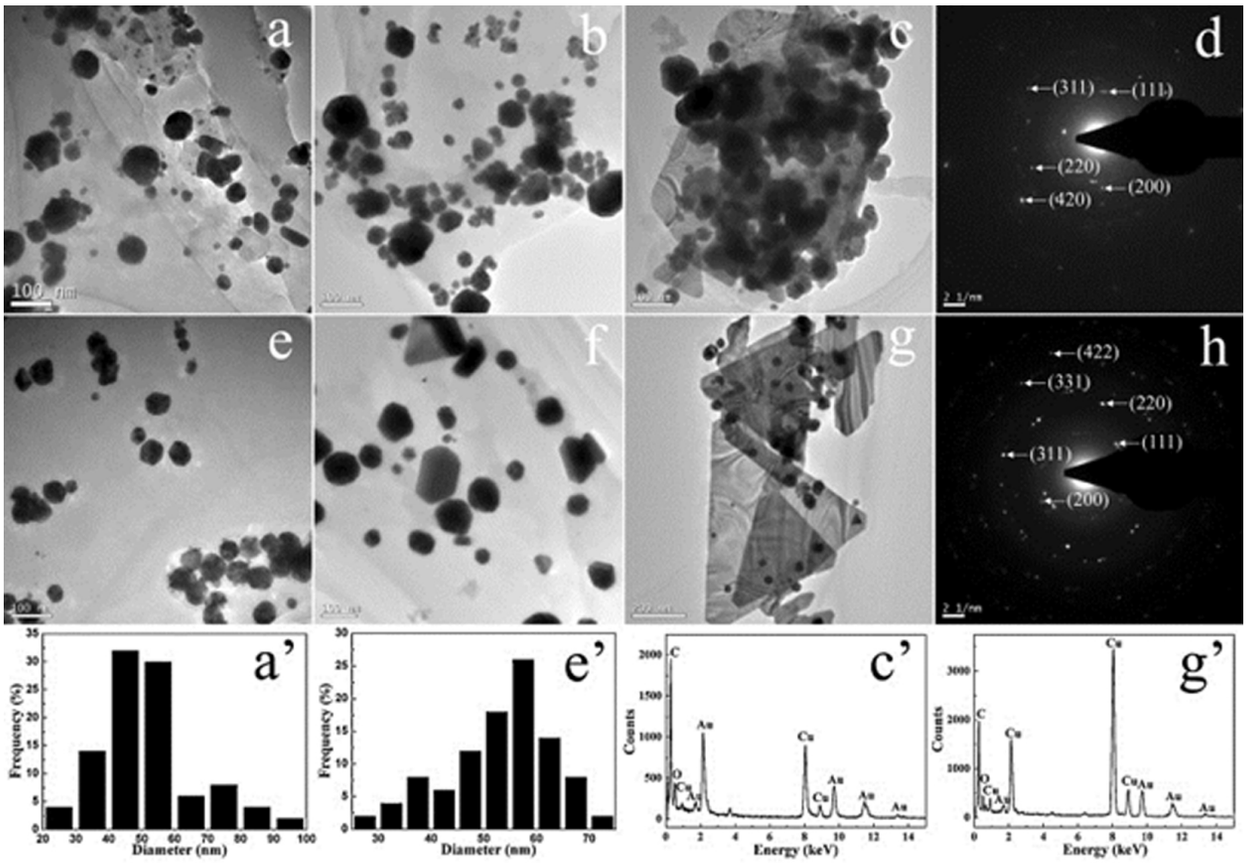


Figure 1. TEM images of gold nanoparticles using NpN1 and NpN2 with different amphiphile to chloroaurate ion ratio of 2:1 (a and e), 1:1 (b and f) and 1:2 (c and g) after 35 h, respectively. (d and h) SAED pattern and (c′ and g′) EDXS taken on the gold nanoparticle shown in (c and g), respectively. The Cu peaks originate from the TEM grid. (a′ and e′) Particle size distribution histograms of gold nanoparticles from TEM images (a and e), respectively.

could serve as both capping and reducing agents. Different gold nanostructures could be obtained depending on the different spacers and the molar ratios of amphiphile to $AuCl_4^-$ ions. In order to investigate the gold nanostructures, the chloroform solution was cast onto copper grid for TEM measurement, as shown in Figure 2. Two main results were obviously observed. One was the particle size distribution of gold nanostructures that changed distinctly depending on the different spacers in two bolaform amphiphiles. Another was the effect of molar ratio of the amphiphiles to $AuCl_4^-$ ions on the generation of gold nanostructures. In addition, we also researched the effect of molar ratio of the amphiphiles to $AuCl_4^-$ ions on the creation of gold nanostructures. The experimental results showed that, with the increase of molar ratio of the compounds to $AuCl_4^-$ ions from 2:1 to 1:2, different kinds of shapes and nanostructures were gained, including hexagonal, polygon nanoparticles and nanoplates with larger size, respectively. The obtained data demonstrated excess bolaform amide compounds could significantly increase the reducing ability, and the rapid reduction usually produced larger nanostructures and nanoparticles. In addition, the photocatalytic performances of as-prepared gold nanostructures on the degradation of dye (methyl orange as example) demonstrated that the spacers in the compounds skeletons indeed played an important role in regulating the sizes of obtained gold nanoparticles and subsequently changing relative catalytic behaviors. The

http://dx.doi.org/10.5772/60796

obtained research results would provide an exploratory investigation about the design and preparation of gold nanostructures by utilizing bolaform compounds with different skeletons and spacers.

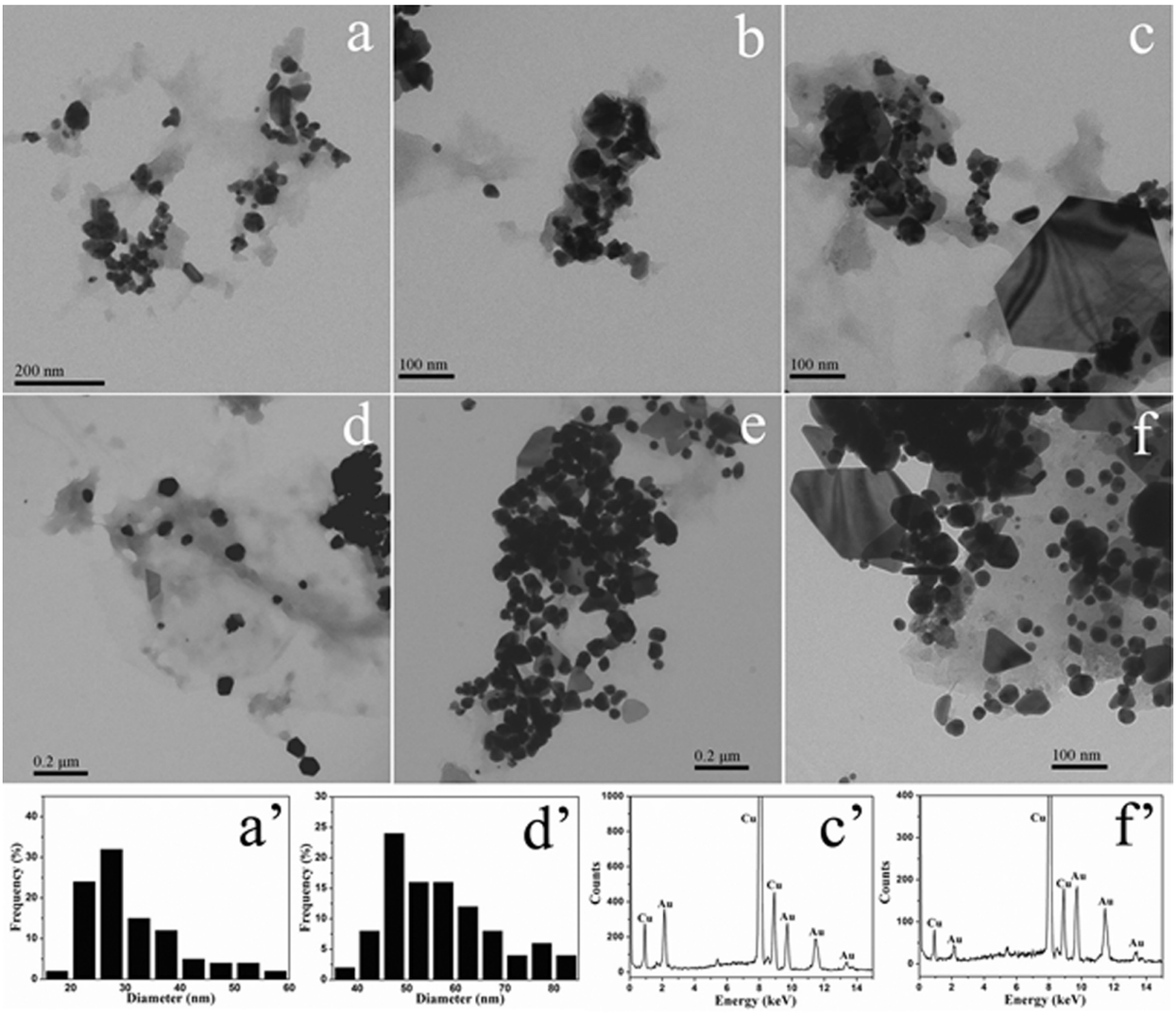
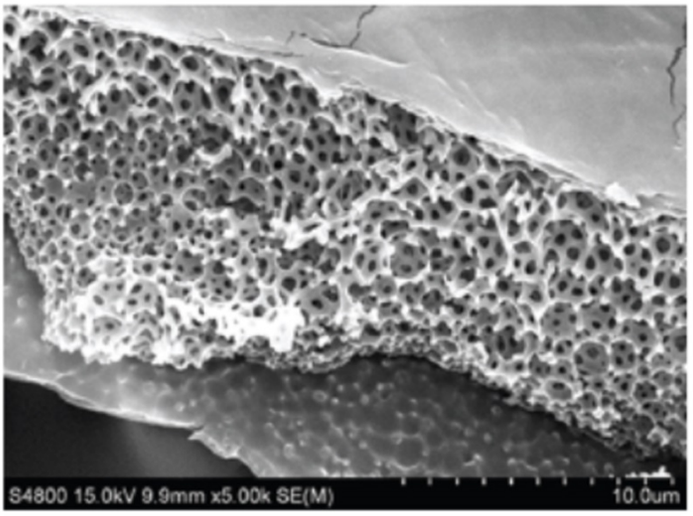


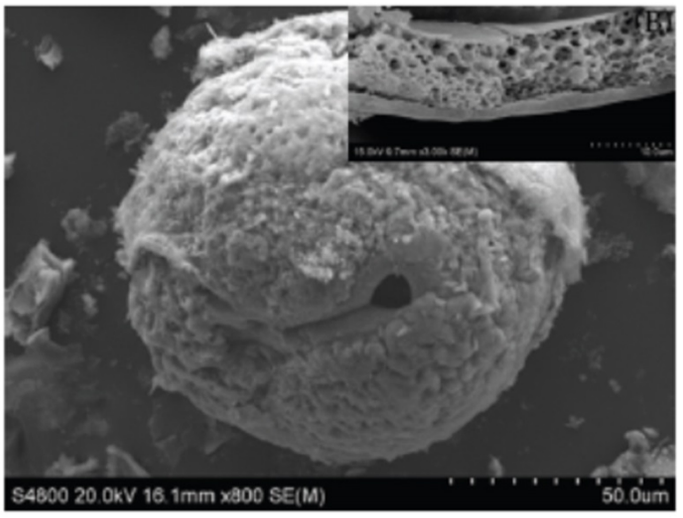
Figure 2. TEM images of gold nanoparticles using CH-N1 and CH-N2 with different amphiphile to chloroaurate ion ratio of 2:1 (a, d), 1:1 (b, e), and 1:2 (c, f) after 35 h, respectively. (c′, f′) EDXS were taken on the gold nanoparticle shown in (c and f), respectively. The Cu peaks originate from the TEM grid. (a′, d′) Particle size distribution histograms of gold nanoparticles from TEM images (a, d), respectively.

Moreover, composites of the nano-sized perovskite-type oxide of $LaMnO_3$ and multi-walled carbon nanotubes (MWCNTs) were synthesized in a single step using the sol–gel method [24]. Their photocatalytic activities for the degradation of various water-soluble dyes under visible light were evaluated. The prepared samples were characterized by thermogravimetry analysis, scanning electron microscopy, transmission electron microscopy, X-ray diffraction, photoluminescence spectroscopy, and UV–vis diffused spectroscopy. Results showed that $LaMnO_3$ nanoparticles grew on the surface of MWCNTs with a grain size of around 20 nm. Photoca-

talysis measurements revealed that the $LaMnO_3$/MWCNT nanocomposites had greater photocatalytic activities than pure $LaMnO_3$ nanoparticles, and the mass percentage of MWCNTs showed that 9.4% possessed the highest photocatalytic activity. These results can serve as a foundation for further research on developing MWCNTs-hybridized materials and improving the photocatalytic activity of the perovskite-type structure photocatalyst.



(a)



(b)

Figure 3. SEM images of (a) neat Artemia egg shell and (b) the shell–TiO2 composite material.

In another research system, some Artemia egg shell with asymptotic reduction pores (diameter: 500–2500 nm, shown in Figure 3) can be used as the carrier for nanocomposite materials [25]. The nanocomposite materials, Artemia egg shell-supported TiO_2, were in polycrystalline-like nanostructures and can be used for high-efficiency formaldehyde removal under visible light. Our results would suggest that iron, as one of the shell's natural components, should be

http://dx.doi.org/10.5772/60796

associated with the photocatalytic performance of shell–TiO_2 composites. Due to their interesting absorption and formaldehyde removal qualities, Artemia egg shell, as a novel naturally porous carrier for nanocomposite materials preparation, especially in the preparation of nanocatalysts, is worthy of further study.

In addition, a new hybrid nanocomposite was prepared by encapsulating ZrO_2 nanoparticles into spherical polystyrene beads (MPS) covalently linked with charged sulfonate groups ($-SO_3^-$) [26]. The obtained adsorbent material, Zr–MPS, demonstrated more preferential sorption performance toward Pb(II) than the simple equivalent mixture of MPS and ZrO_2. Such experimental data might be assigned to the hybrid of sulfonate groups in polymeric host spheres, which could increase nano-ZrO_2 dispersion and Pb(II) diffusion performances. In order to investigate the effect of surface functionalized groups, we composite nano-ZrO_2 with another two macroporous polystyrene host materials with different surface groups (i.e., $-N(CH_3)_3^+$/$-CH_2Cl$, respectively) and a conventional activated carbon, as shown in Figure 4. The three obtained nanocomposites were abbreviated as Zr–MPN, Zr–MPC, and Zr–GAC. The presence of $-SO_3^-$ and $-N(CH_3)_3^+$ was more favorable for nano-ZrO_2 dispersion than the neutral $-CH_2Cl$, resulting in the sequence of sorption capacities as Zr–MPS > Zr–MPN > Zr–GAC > Zr–MPC. Present study suggests that charged groups in the host resins improve the dispersion of embedded nanoparticles and enhance the reactivity and capacity for sorption of metal ions. In addition, selection of suitable surface groups is also a key factor related to the sorption kinetic enhancement and sorption performance for application.

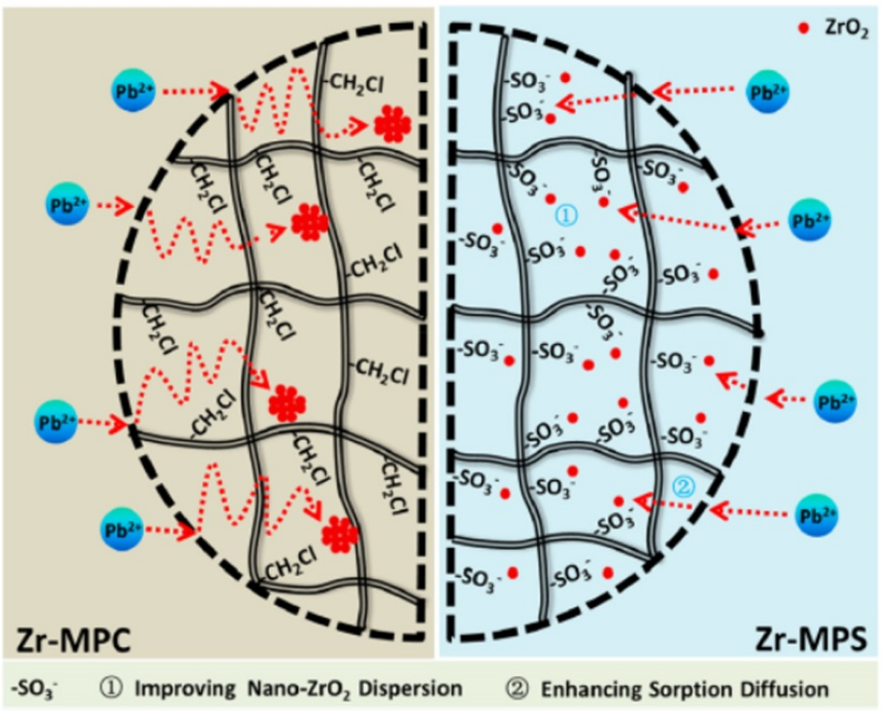


Figure 4. Schematic illustration of the role of charged sulfonate groups of polymeric host on the properties of Zr–MPS toward Pb(II) retention ($-CH_2Cl$ was involved for comparison purpose).

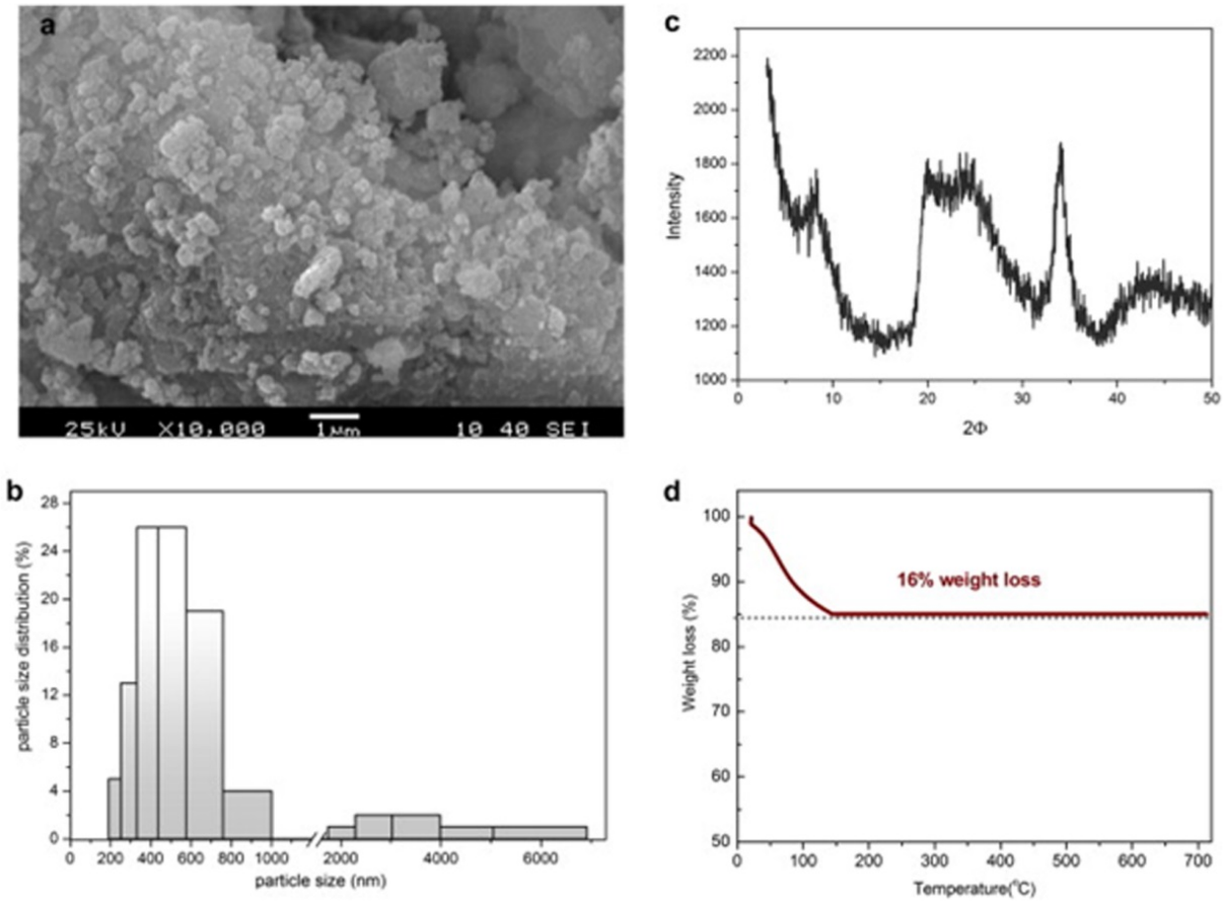


Figure 5. Characterization of ZrP particles (a) SEM of ZrP; (b) ZrP particles size distributions by DLS analysis; (c) XRD analysis of ZrP; (d) TGA curve of ZrP.

In another study, amorphous zirconium phosphate (ZrP) was prepared and the increased sorption performances toward anion-phosphate were investigated [27]. The uptake of phosphate onto ZrP was measured, and the common used anion-exchange resin (D201) and zirconium dioxide particles were introduced for references with coexistence of common anions, the results indicated that both ZrP and ZrO_2 exhibited more favorable sorption performances than D-201, which might be ascribed to the information of inner-sphere complex. Characterizations of ZrP particles were shown in Figure 5. Moreover, the exhausted ZrP particles were amenable to efficient regeneration by alkaline solution for repeated use. All the results rendered us to believe that ZrP is a promising adsorbent for enhanced phosphate removal from contaminated waters.

In addition, nano-ZrP supported by macroporous polystyrene beads with quaternary ammonium groups modification is fabricated based on Donnan membrane principles for efficient fluoride ion removal in waters [28]. The as-obtained materials exhibited favorable removal of fluoride ions from aqueous solution in the presence of common anions (SO_4^{2-}/NO_3^-/Cl^-) at high contents. Such satisfactory performances might be ascribed to the structural design of nanocomposite. Characterizations of the nanocomposite ZrP-MPN were shown in Figure 6. The $CH_2N^+(CH_3)_3Cl$ groups enhance sorption diffusion and preconcentration in sorbent phase

http://dx.doi.org/10.5772/60796

theoretically based on Donnan membrane principle. And the embedded ZrP nanoparticles also devote to the efficient adsorption capacities due to its size-dependent specific properties. Thus, ZrP-MPN was a promising material for fluoride retention in waters.

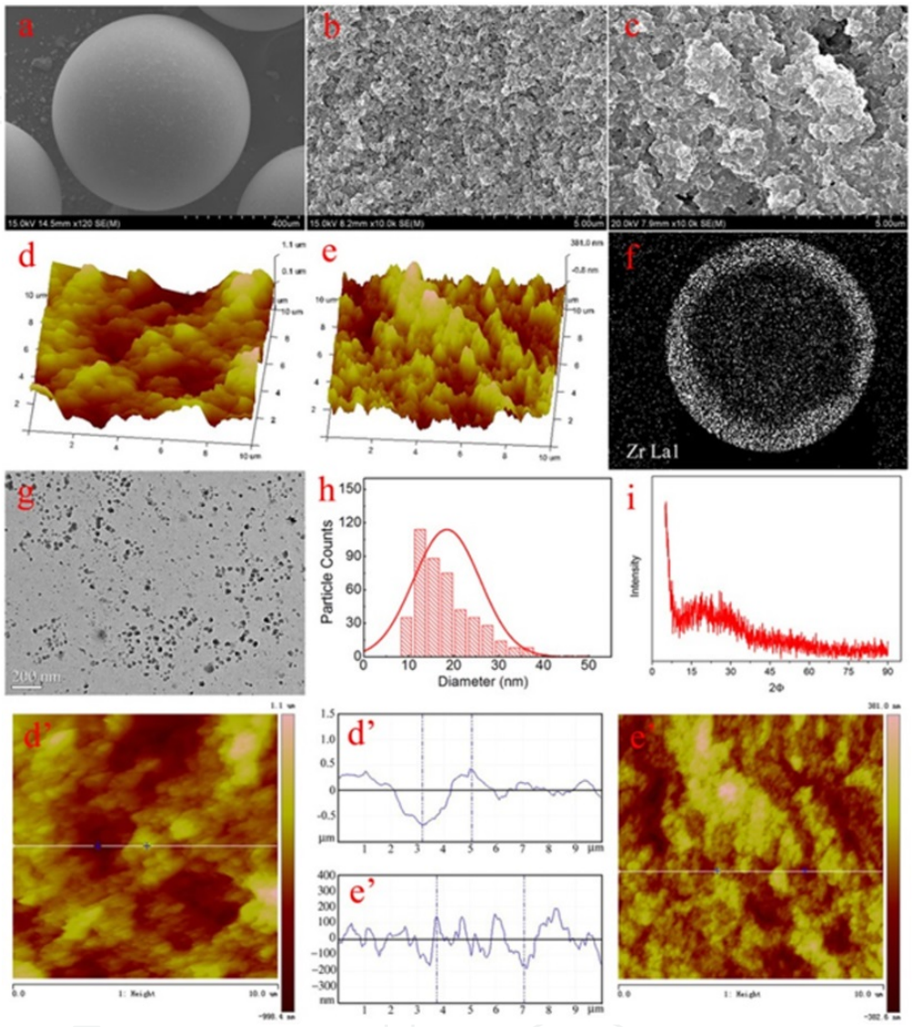


Figure 6. Morphological characterization of the obtained nanocomposites. SEM of (a) spherical bead Zr-MPN, (b) inner surfaces within the host material MPN, (c) inner surfaces within Zr-MPN, AFM 3D analysis onto the inner surface of MPN (d) and ZrP-MPN (e), (f) cross-section Zr distribution of ZrP-MPN by SEM–EDS, (g) TEM of Zr-MPS, (h) the encapsulated ZrP nanoparticle size distribution, (i) XRD spectrum of ZrP-MPN. (d′) AFM line profile analysis of MPN; (e ′) AFM line profile analysis of ZrP-MPN.

Recently, we present a new strategy for a one-step preparation of macroscopic peptide–inorganic hybrid supramolecular films with functionality [29]. The strategy is closely associated with supramolecular interactions of self-assembled starting materials. A mechanism regarding the morphological transition from hybrid nanospheres to visible macroscopic films is proposed, as shown in Figure 7. Firstly, cationic dipeptides and POM anions interact in bulk solution and form PECs as the basic building units mainly through electrostatic attraction. Subsequently, the preformed PECs further stack to form supramolecular networks through hydrophobic interactions, van der Waals forces, and aromatic stacking, finally leading to the

assembly of hybrid nanospheres in water. Depending on the NIR light irradiation, the morphological transition occurs from hybrid nanospheres to visible macroscopic films through a process involving disassembly in the aqueous solution and reorganization at air–water interfaces. Significantly, PECs as basic building blocks remain in the case of the film. The method presented in this study could be extended for preparation of macroscopic films involving weak intermolecular interactions suffering from environmental variations such as temperature and pH, etc.

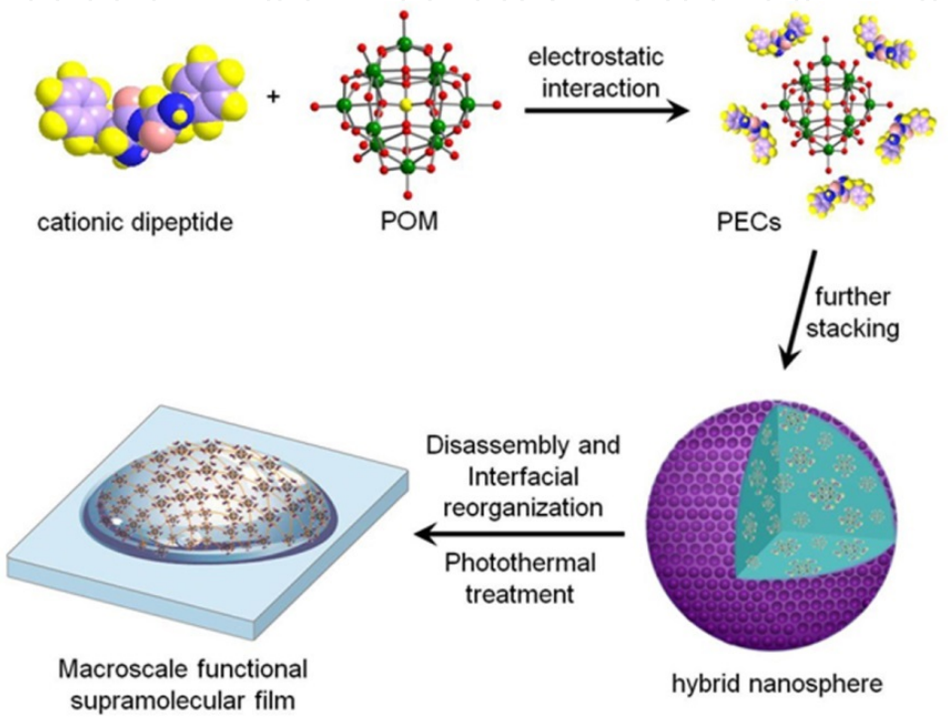


Figure 7. Schematic illustration of the formation of macroscale functional supramolecular films supported onto a solid substrate: hybrid nanospheres are initially self-assembled in aqueous solution mainly by strong electrostatic attraction of cationic dipeptide and polyanions; Structural transformation of a nanosphere solution into the macroscopic film occurs by photothermal treatment, presumably due to photothermally triggered disassembly, and interfacial enrichment and reorganization of PECs.

3. Preparation and self-assembly of some graphene oxide nanocomposites

Graphene, a single layer of sp^2-bonded carbon atoms, is now promising for enhancing photocatalytic activity because of its excellent adsorption capacity, high chemical stability, and large specific surface area [30]. Thus, compounding graphene with semiconductor photocatalysts to develop novel nanocomposites with enhanced photocatalytic performance has received increasing attention. Ullah and coworkers reported that Pt-graphene/TiO_2 nanocomposites were prepared by facile and fast microwave-assisted method and the photocatalytic activities were investigated by the degradation of rhodamine B (Rh.B) as a standard dye [31].

http://dx.doi.org/10.5772/60796

Bai et al. developed $ZnWO_4$/graphene hybrid (GZW-X) photocatalysts by an easy in situ reduction of graphene oxide and $ZnWO_4$ in water and high efficiency for the degradation of methylene blue under both UV and visible light [32]. Sun and coworkers prepared $ZnFe_2O_4$/ZnO nanocomposites immobilized on different content of graphene on the basis of an ultrasound-aided solution method [33]. The molar ratio of $ZnFe_2O_4$ to ZnO and the content of graphene could be controlled by adjusting the amount of zinc salts and graphene oxide dispersions. Xu et al. obtained reduced graphene oxide/Bi_2WO_6 (RGO–Bi_2WO_6) composite photocatalysts, and an enhancement in photocatalytic activities were observed in RGO–Bi_2WO_6 composites compared with pure Bi_2WO_6 [34]. To enhance the photocatalytic activity, efforts have been exerted to load photocatalysts on the structure of graphene [35–38]. In this part, we have demonstrated some examples of research systems including preparation of magnetite/reduced graphene oxide (MRGO) nanocomposites for removal of dye pollutants, as well as metal oxides–graphene composite for photocatalyst. These works not only provided important inspirations for developing graphene-hybridized materials but also opened new possibilities to improve the photocatalytic activity of photocatalyst.

Firstly, $LaMnO_3$-graphene nanocomposite photocatalysts were synthesized by a sol–gel method for the first time [39]. Pure $LaMnO_3$ perovskite phase was successfully anchored on the surface of graphene sheets and had good dispersion behavior, as shown in Figure 8. The photocatalytic activity of the $LaMnO_3$–graphene composite was higher than that of the pristine $LaMnO_3$. The enhancement of UV–vis photocatalytic light activity can be attributed to the high separation efficiency of photo-induced electron–hole pairs resulting from the excellent conductivity of graphene in $LaMnO_3$–graphene and the large surface contact between graphene and $LaMnO_3$, which can promote the adsorption of organic dyes and improve the transfer efficiency of the photocatalytic process. This work not only provided important inspirations for developing graphene-hybridized materials but also opened new possibilities to improve the photocatalytic activity of perovskite photocatalyst.

In another research work, $La_{1-x}Sr_xMnO_3$/graphene thin films were obtained using sol–gel and spin-coating methods on glass substrates [40]. A combination of chemical bonds between the thin films and substrates was achieved using a silane coupling agent (APTES), illustrated in Figure 9. In this method, the sol particles were adsorbed on the graphene surface by electrostatic adsorption in aging stage. The subsequent calcination process made the $LaMnO_3$ particles grow and crystallize on the graphene surface. The structure, grain size, and morphology were characterized by spectral and morphological methods. Results show that perovskite nanoparticles grew on graphene, and the size of the grain was about 40 nm. In the process of acid red 3GN photodegradation, $LaMnO_3$/graphene thin film had sound stability and better photocatalytic ability than $LaMnO_3$ thin film. Graphene accelerated the adsorption of the dye, which inhibited the reunion of light-induced e^-–h^+, and improved the photocatalytic efficiency. A red shift of the absorption edge, which enhanced the photocatalytic performance of the $LaMnO_3$/graphene thin film, was achieved by doping Sr. When $x = 0.1$, the decoloration rate reached 94.52%, and the TOC concentration of acid red 3GN was only 0.36 mg/L after illumination for 4 h.

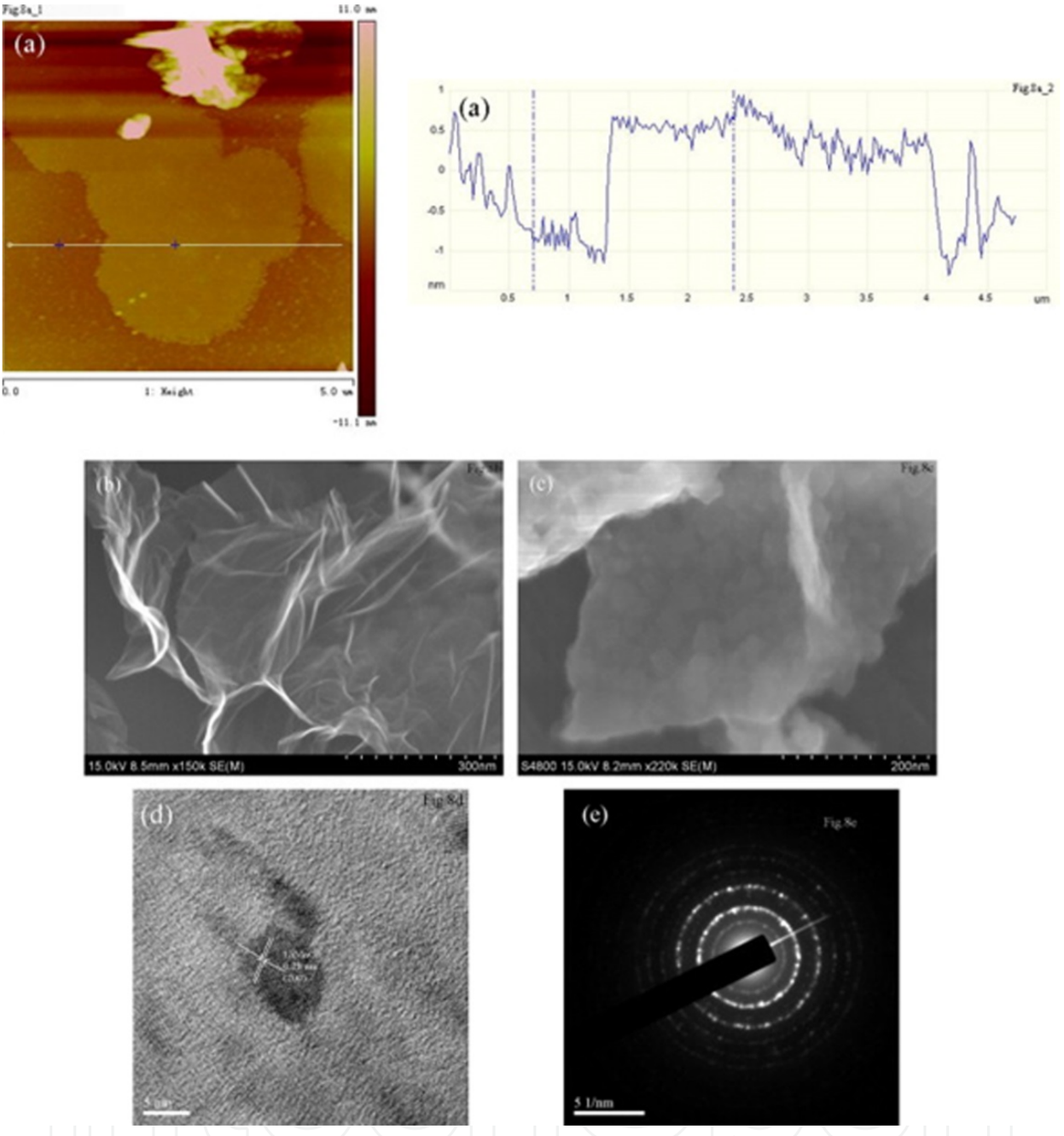


Figure 8. (a) AFM image of the as-synthesized graphene; (b) SEM image of graphene; (c, d, e) SEM, HRTEM and SAED images of $LaMnO_3$-graphene composites.

In addition, a novel photocatalyst of $LaMn_{1-x}Co_xO_3$/graphene composites had been synthesized by sol–gel process assisted with chelating effect of citric acid [41]. It was found that $LaMnO_3$ perovskite phase was successfully processed which anchored on the surface of graphene sheets, and doping Co did not change the perovskite structure. The UV–vis photocatalytic activity of the photocatalysts was evaluated by the degradation of diamine green B. In the photodegradation of diamine green B, after graphene was introduced to $LaMnO_3$ as a photocatalytic, it can accelerate the adsorption of the dye, while doping Co enhances the photoca-

http://dx.doi.org/10.5772/60796

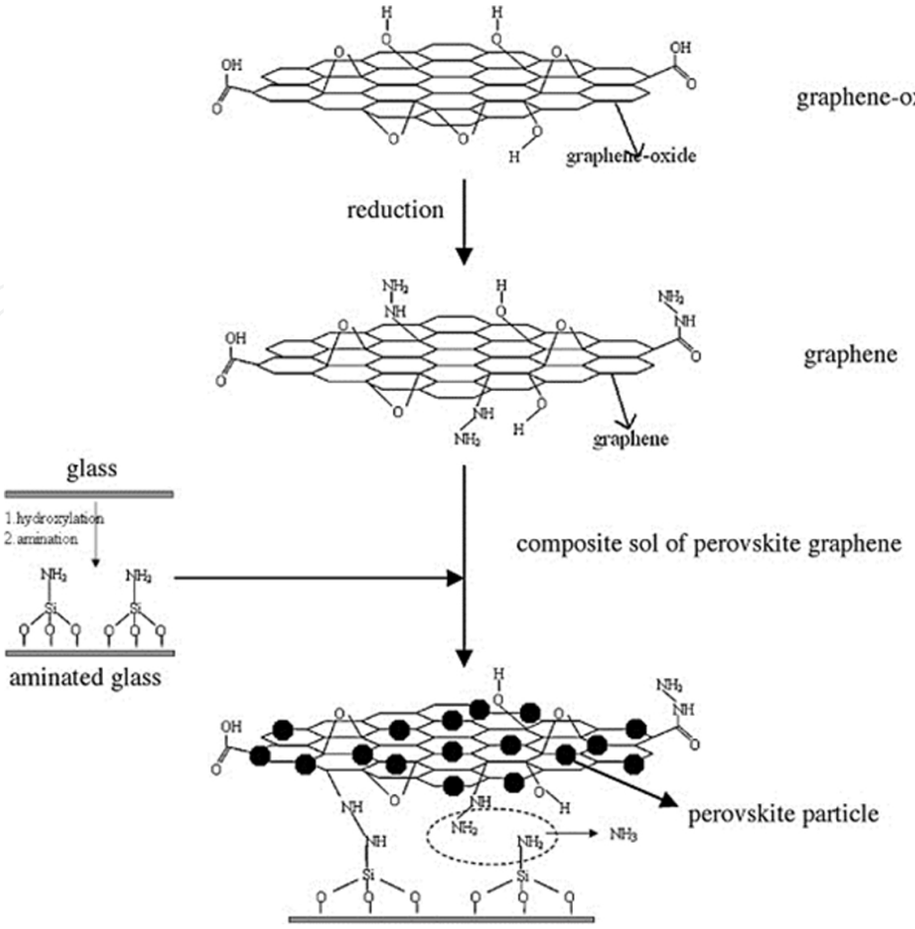


Figure 9. Preparation flow chart of the $LaMnO_3$/graphene thin film on glass substrate.

talytic performance of $LaMnO_3$/graphene composites and $LaMn_{0.85}Co_{0.15}O_3$/graphene composite has the best catalytic activity. The charge transfer mechanism that occurs in the $LaMnO_3$/graphene composite during photocatalytic process is shown in Figure 10. Diamine green B molecules could transfer from the solution to the composites' surface and be adsorbed with offset face-to-face orientation via π–π conjugation between diamine green B and aromatic regions of the graphene; therefore, due to its giant π-conjugation system and two-dimensional planar structure, the adsorptivity of dyes improved compared to the bare $LaMnO_3$. Due to these holes and electron transfers, charge recombination is suppressed in $LaMnO_3$/graphene composite and hence largely enhances the efficiency of photocatalytic properties.

Moreover, some graphene-based $LaNiO_3$ composite films were also prepared by using sol–gel method and spin coating technique on glass substrate [42]. The composite films were characterized by various techniques. The experimental data demonstrated that the size of $LaNiO_3$ crystalline grains is about 20 nm with uniform growth in graphene sheet. The photocatalytic performance of films had been investigated by degradation of Acid red A as an example. Comparing with $LaNiO_3$ films, the $LaNiO_3$/graphene composite films indicated better photocatalysis properties. When the content of graphene is changed as about 4%, the photocatalytic efficiency of the $LaNiO_3$/graphene composite films is double of the $LaNiO_3$ films.

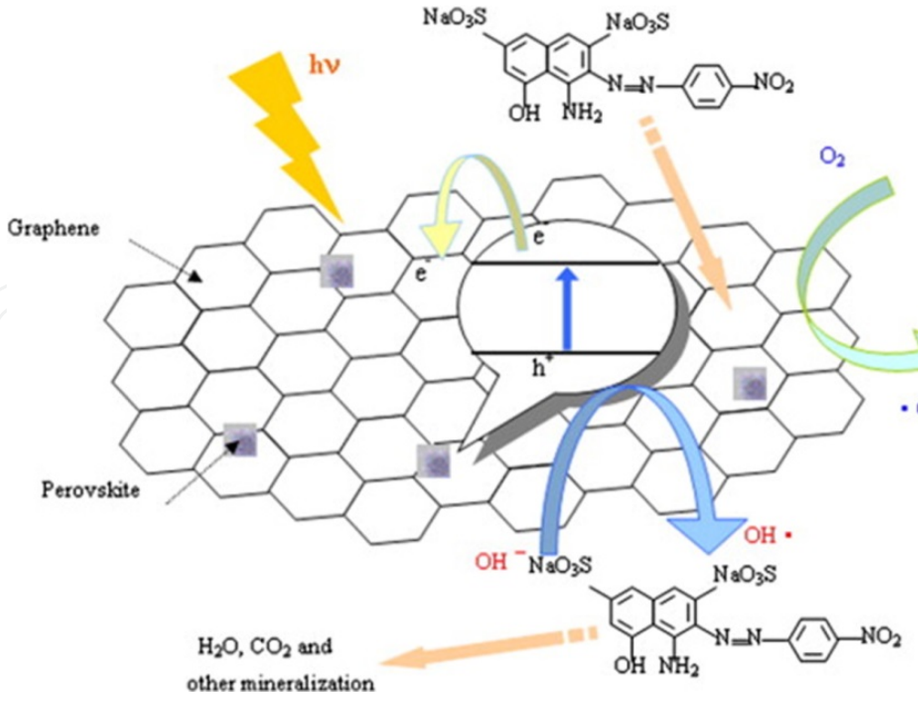


Figure 10. Proposed mechanism for photocatalytic degradation of diamine green B over graphene-based perovskite photocatalysts under light irradiation.

In another system, $La_{1-x}Ca_xMnO_3$ perovskite–graphene composites are synthesized as catalysts for Zn–air cell cathodes [43]. The results indicated that perovskite phase adhered on the surface of graphene sheets, and adding graphene significantly improved the electrochemical performance of $LaMnO_3$. FE-SEM analyses were carried out to observe the morphology of the as-synthesized material, as shown in Figure 11. The as-prepared graphene have gauze-shaped wrinkles and folds structure, which may be caused by oxygenic functional group and the resultant defects during the preparation of graphene oxide. As catalyst of air electrode, its porous structure could greatly increase the three-phase region, thereby improving the mass transfer process. The voltage plateau was superior when the ratio of graphene was 10 wt%. Ca doping not only maintained the perovskite structure but also significantly improved the electrocatalytic activity for the ORR, and $La_{0.6}Ca_{0.4}MnO_3$–graphene exhibited the best catalytic activity. The electron transfer number of $La_{0.6}Ca_{0.4}MnO_3$–graphene was 3.6, which was calculated from the RRDE measurement result. This finding indicated that the sample exhibited considerable catalytic activity for the ORR. These results indicate that the $La_{1-}xCaxMnO_3$–graphene composites are potential air electrodes catalysts.

Recently, a new photocatalyst of $LaMnO_3$/graphene thin films with the perovskite-type was synthesized by sol–gel process assisted with spin coating methods on glass substrates [44]. Results showed that after the introduction of graphene, the perovskite structure was unchanged and the size of $LaMnO_3$ particles was about 22 nm, with uniform growth in graphene sheet. Determination of contact angle indicated that the contact angle of glass substrate decreased and the hydrophilicity improved after treating with H_2SO_4 and APTES. The UV-vis photocatalytic activity of the photocatalysts was evaluated by the degradation of diamine

http://dx.doi.org/10.5772/60796

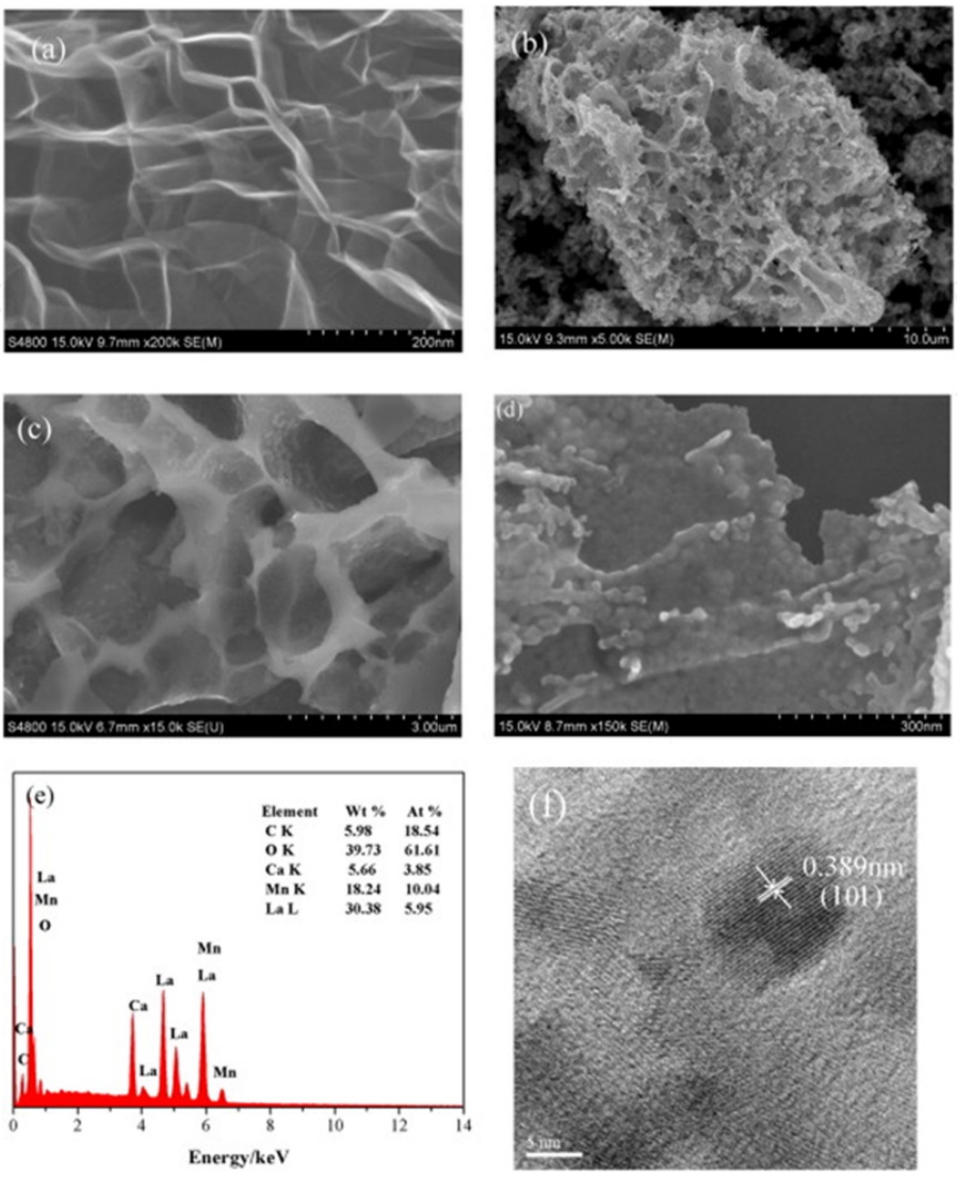


Figure 11. FESEM images of (a) graphene; (b, c, d) FE-SEM, (e) EDS, (f) HRTEM of $La_{0.6}Ca_{0.4}MnO_3$–graphene composite.

green B. $LaMnO_3$/graphene thin films had better photocatalytic ability than $LaMnO_3$ and TiO_2 films.

4. Preparation and self-assembly of supramolecular gels based on some functionalized imide amphiphiles/ binary mixtures

In recent years, supramolecular gels, which show different organized three-dimensional aggregates with micrometer-scale/nanometer-scale lengths and diameters immobilizing the flow of liquids (water or organic solvents), have been well known for wide applications on

drug delivery, functionalized materials, agents, and sensors as well as water purification [45–48]. The driving forces responsible for gel formations are mainly different noncovalent interactions, such as van der Waals forces, hydrogen bonding, dipole–dipole interaction, π–π stacking, and host–guest interaction [49–51]. On the other hand, gels are early investigated in macromolecular/polymer cases, but there has recently been an increasing attention in low molecular mass organic gelators (LMOGs) [52–54]. Such kind of organogels have some advantages over previous polymer-based gels: the molecular structure of the gelator is defined, and the gel process is usually reversible. Such properties can allow to design and prepare various functionalized gel systems and produce more complicated and controllable nanocomposites and/or nanostructures [55–57]. In this part, we have demonstrated some examples of such systems including supramolecular gels based on some functionalized imide amphiphiles or binary mixtures. The gelation properties of these organogels will be discussed to attempt to understand the stacking mechanism and assembly modes and thereby try to control multidirectional self-assembly in some content. The objective is to give some insight to design and character new versatile organogelators and soft materials with special molecular structures.

Firstly, two new cholesterol imide derivatives with azobenzene substituent groups have been synthesized. The difference in the headgroups of azobenzene segment can produce a dramatic change in the gelation behavior [58]. Upon UV irradiation on the as-formed gel, *trans–cis* photoisomerization of the azobenzene functionalized groups occurs, and the shift in molecular polarity leads to the collapsed breaking of van der Waals forces, resulting in the gel–sol transition. In addition, the formed gel can also be recovered by the reverse *cis–trans* photoisomerization after exposure to visible light, as shown in Figure 12. Morphological and spectral results indicate that the gelator molecules self-assemble into one-dimensional belts with diameters 50–80 nm, which further self-assemble to form regular nanobelts. The obtained experimental data give useful information for the development of new functionalized low molecular mass organogelators and nanomaterials.

In addition, new bolaform and trigonal cholesteryl amide derivatives with different aromatic spacers were designed and prepared [59]. The gelation behaviors of two cholesteryl derivatives with aromatic spacers in various organic solvents can be regulated by changing spacer size and molecular shapes, as shown in Figure 13. While the trigonal compound gels 3 of the 20 solvents investigated at a concentration more than 3.0%, the bolaform amide compound gels 2 of the solvents tested at a concentration more than 2.0%, respectively. In addition, morphological observations indicate that the size of the spacers and the identity of the solvents are the main factors affecting the organized stacking of the aggregates in the as-formed gels. After experimental investigation, a clear process about spacer effect on the organized nanostructures of the gels was proposed.

In another study, some new glutamic acid diethyl ester imide derivatives with different alkyl substituent chains were designed and synthesized [60]. The results indicated that the length of alkyl substituent chains linked to benzene ring in gelator compounds played an important role in the gelation performance of all compounds in various organic solvents. Longer alkyl chains in molecular skeletons in the present as-formed gelators are favorable for the gelation

http://dx.doi.org/10.5772/60796

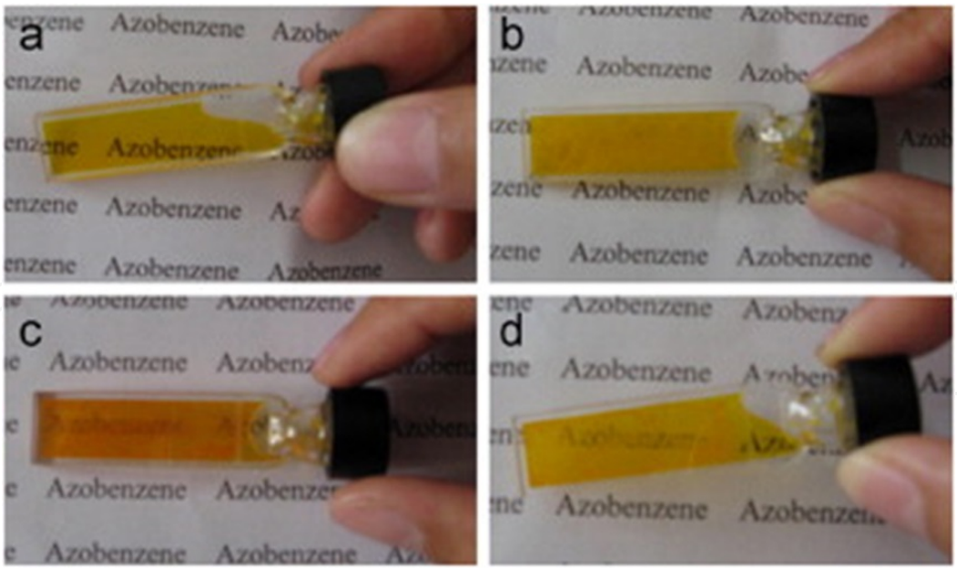


Figure 12. Photographs of Ch-azo (1.5% w/v, 0.1 cm path length) in hot DMF solution (a), formed gel in room temperature (b), after UV irradiation for 170 min (c), and subsequent visible irradiation for 40 min (d).

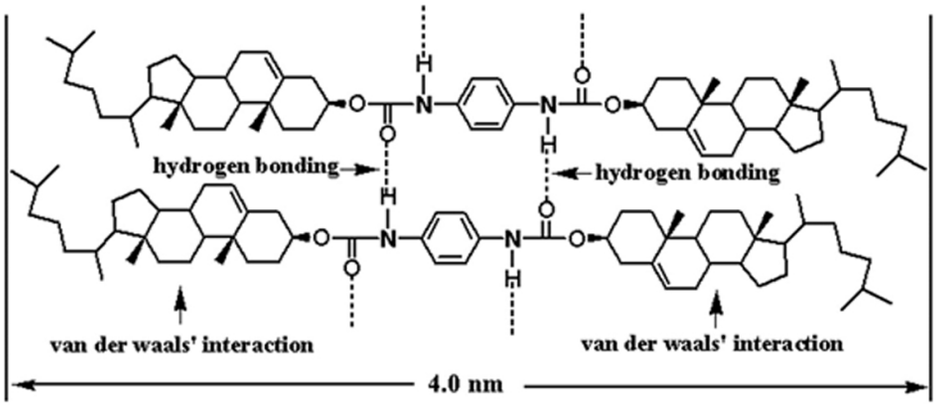


Figure 13. A possible aggregation mode of Ch-p-ben gel in aniline.

of organic solvents. SEM and AFM investigation demonstrated that the gelator molecules self-assemble into different aggregates from wrinkle, lamella, belt, to fiber with change of solvents. In addition, the xerogels in nitrobenzene of all compounds were characterized by AFM, as shown in Figure 14. From the pictures, it is wealthy to note that these big belt or lamella aggregates contained many little domains by stacking of the present imide compounds. Spectral studies indicated that there existed different H-bond formations and hydrophobic forces, depending on the alkyl substituent chains in molecular skeletons.

In addition, four azobenzene imide derivatives with different substituent groups were designed and synthesized. Their gelation behaviors in 21 solvents were tested as novel low-molecular-mass organic gelators [61]. It was shown that the substituent groups in azobenzene residue and benzoic acid derivatives can have a profound effect upon the gelation abilities of

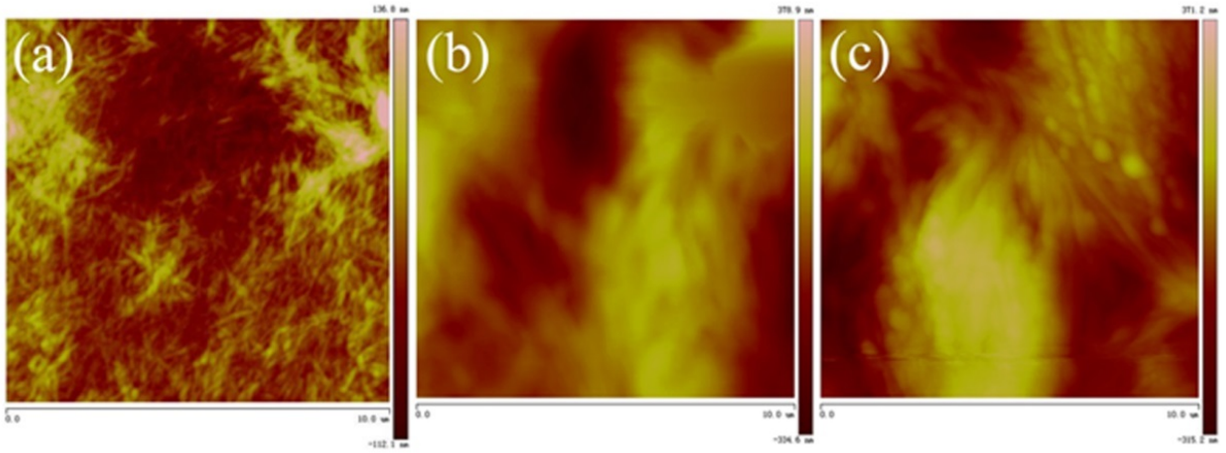


Figure 14. AFM images of xerogels from GC16 (a), GC14 (b), and GC12 (c) gels in nitrobenzene, respectively.

these studied compounds. The results indicated that more alkyl chains in compound skeletons in the present used gelators are favorable for the gelation of organic solvents. Morphological investigations suggested that the gelator molecules self-assemble into different shapes of aggregates, from wrinkle, lamella, and belt to fiber with the change of solvents, as shown in Figure 15. The present work may give some insight to the design and character of new organogelators and soft materials with special molecular structures.

It is well known that luminol is regarded as a famous and efficient case in electrochemiluminescence (ECL) investigations for the detection of hydrogen peroxide. In our previous reports, some novel luminol imide compounds with various substituent alkyl chains were designed and prepared. Their gelation performances in 26 solvents were measured as new low molecular mass organic gelators [62]. The experimental data indicated that the length and substituent number of alkyl chains connected with benzene ring in gelator skeletons played an important role in the gelation formation of all imide derivatives in different organic solvents. Longer alkyl chains in molecular structures in used gelator compounds are favorable for the gelation of present organic solvents. Morphological investigations suggested that the gelator molecules self-assemble into various micro/nanoscale aggregates from dot, flower, belt, rod, and lamella to wrinkle with solvents change, as shown in Figure 16. Considering the XRD results described above and the hydrogen bonding nature of the orderly aggregation of these imide compounds as confirmed by FT-IR, a possible assembly mode of TC18-Lu organogels was proposed. Now the ECL properties generated by the present xerogels of these luminol derivatives in the presence of hydrogen peroxide are under investigation to display the relationship between the molecular structures, as-formed nanostructures, and ECL sensors.

In addition, some functional cholesteryl compounds with various spacers were chosen and prepared. Their gelation performances in 23 solvents were tested, and some of them were investigated to be low molecular mass organic gelators [63]. The obtained data suggested that these as-prepared organogels can be changed by regulating the flexible/rigid parts in spacers and organic solvents. Suitable joint of flexible/rigid parts in molecular spacers in the used cholesteryl compounds is favorable for the gelation of organic solvents. To obtain a visual

http://dx.doi.org/10.5772/60796

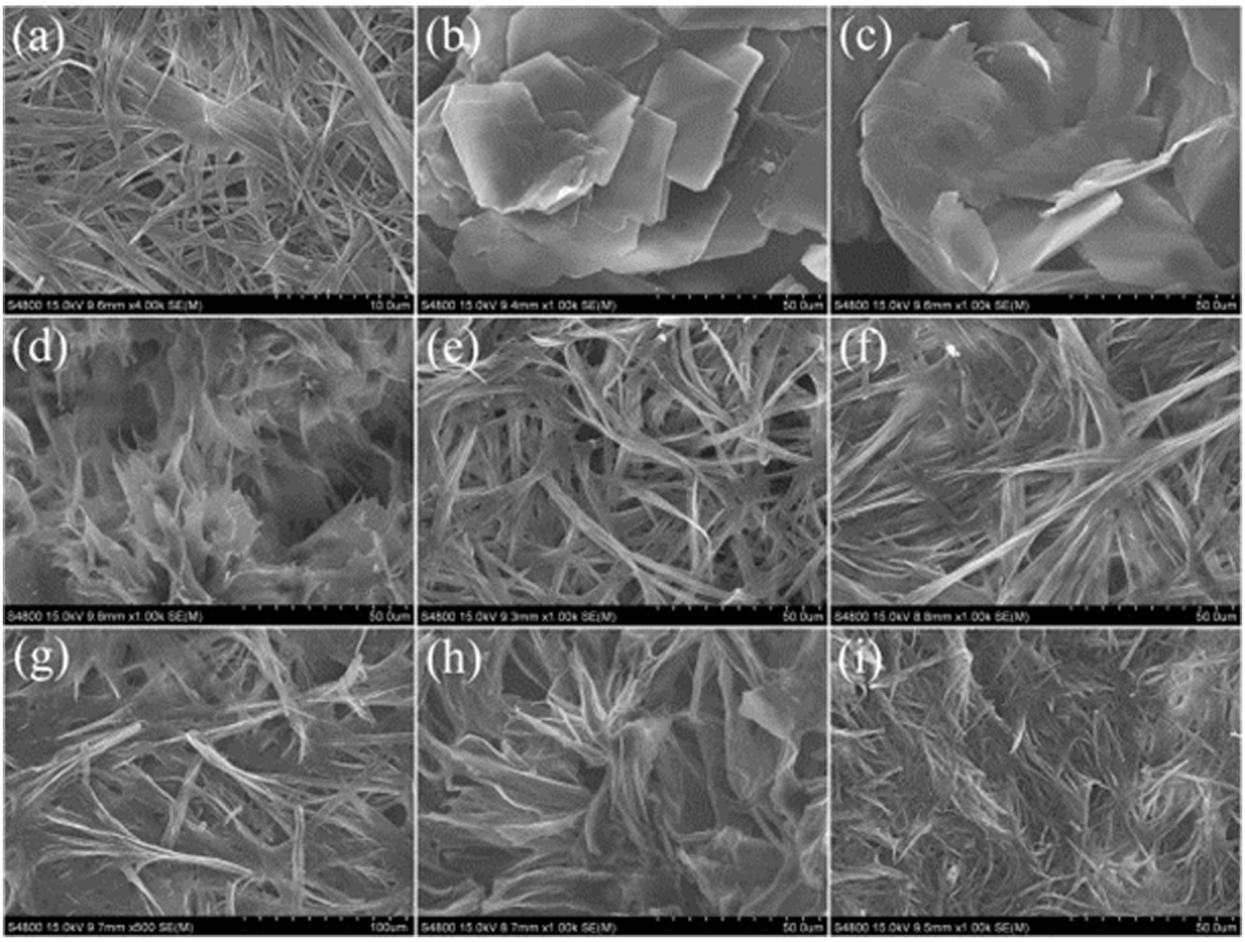


Figure 15. SEM images of xerogels. SC16-Azo gels ((a) benzene, (b) pyridine, and (c) DMF) and SC16-Azo-Me gels ((d) tetrachloromethane, (e) benzene, (f) nitrobenzene, (g) aniline, (h) DMF, and (i) 1,4-dioxane).

insight into the prepared gel nanostructures, the typical nanostructures of these gels were investigated by SEM technique, as shown in Figure 17. Considering the obtained results and the interaction nature about organized stacking in prepared organogels, some reasonable stacking modes in the formed gelators were proposed. As for CH-C1 xerogel from 1,4-dioxane, due to the flexibility of ether band in the molecular structures and various intermolecular forces with solvents, after the oriented hydrogen bonding and organized stacking in different solvents, various stacking units with various lengths were gained. As for CH-C3 with an additional diphenyl part connected with ether band in the spacer segment, the joint of a flexible ether band and a rigid diphenyl part in the molecular spacer with π–π stacking seemed more suitable to regulate molecular conformation to self-assemble and form organized self-assembly nanostructures. On the other hand, for the case of CH-C4 with a five-carbon alkyl substituent chain connected with phenoxy ether band in the molecular spacer, due to the addition of a flexible alkyl segment and a weak hydrophobic force between alkyl chains, it can also self-assemble to fabricate some belt-like domains. Moreover, for CH-C2 and CH-N1, the inefficient or poor gelation behaviors in used solvents may be mainly attributed to the too rigid or too flexible spacers in molecular skeletons, which cannot cause enough intermolecular forces to

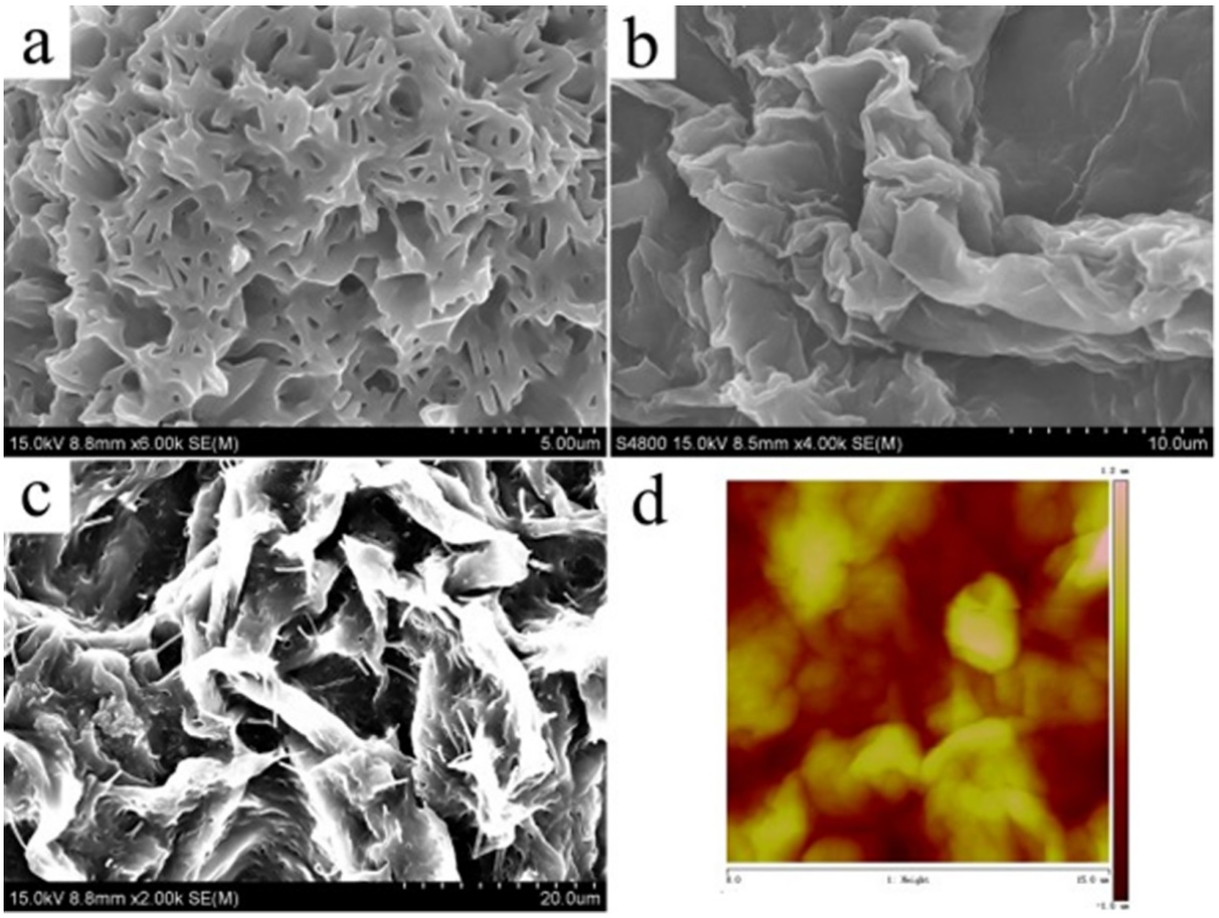


Figure 16. SEM and AFM images of xerogels. (a) TC18-Lu, (b,d) TC16-Lu, and (c) TC14-Lu in DMF gels.

make the molecules align and self-assemble in an organized way to form various nanostructures. Now, the drug release behaviors generated by the present xerogels in the mixture of Congo red are under investigation to display the relationship between the molecular structures of as-formed nanostructures and their properties.

Moreover, another bolaform cholesteryl imide derivative with conjugated aromatic spacer was designed and prepared. The gelation performances in 23 solvents were tested as efficient low-molecular-mass organic gelator [64]. The obtained data demonstrated that the morphologies and assembly modes of as-prepared organogels can be changed by regulating different kinds of organic solvents. Considering the described experimental results, some possible assembly mechanisms about the gelators were proposed and schematically shown in Figure 18. As for CH-PY xerogel from n-butyl acrylate, due to the rigidity of conjugated spacer in molecular structure and different intermolecular forces with solvents, after oriented hydrogen bonding and orderly π–π stacking, CH-PY molecules have a tendency to self-assemble in stretched mode. As for CH-PY xerogels from used other solvents, such as n-pentanol and cyclopentanone, in comparison with π–π stacking, the intermolecular forces with solvents seemed more obvious to adjust molecular conformation to self-assemble and form different twisted stacking nanostructures.

http://dx.doi.org/10.5772/60796

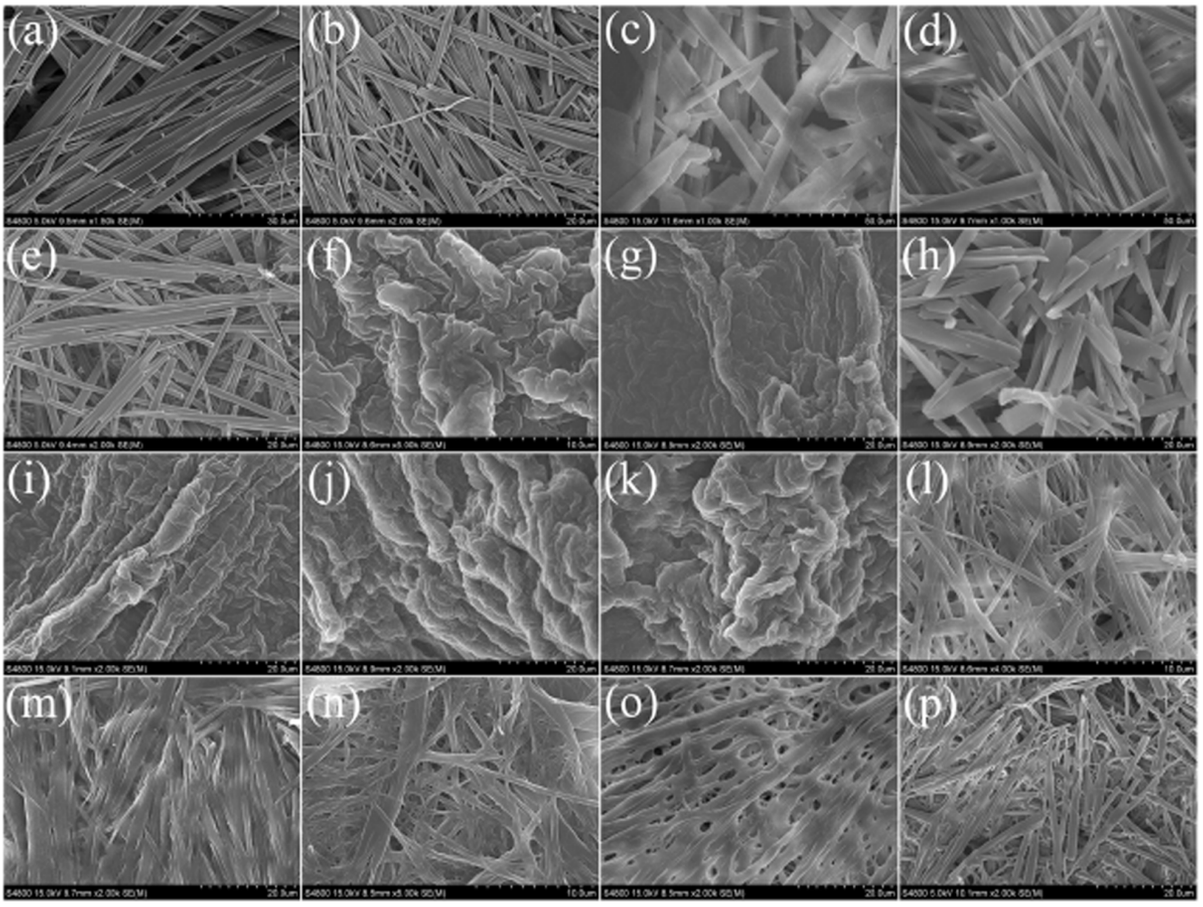


Figure 17. SEM images of xerogels. CH-C1 gels ((a) isooctanol, (b) n-hexane, (c) 1,4-dioxane, (d) nitrobenzene, (e) aniline), CH-C3 gels ((f) cyclohexanone, (g) 1,4-dioxane, (h) nitrobenzene, (i) ethyl acetate, (j) petroleum ether, (k) DMF), CH-C4 gels ((l) nitrobenzene, (m) aniline, (n) n-butyl acrylate, (o) DMF), and CH-N1 gels ((p) pyridine).

In another research work, the gelation behaviors of binary organogels composed of azobenzene amino derivatives and alkyloxybenzoic acids with different lengths of alkyl chains in various organic solvents were investigated and characterized [65]. The corresponding gelation performances in 20 solvents were characterized and shown as novel binary organic systems. It indicated that the lengths of substituent alkyl chains in compounds have played an important role in the gelation formation of gelator mixtures in present tested organic solvents. Longer methylene chains in molecular skeletons in these gelators seem more suitable for the gelation of present solvents. Morphological characterization showed that these gelator compounds have the tendency to self-assemble into various aggregates from lamella, wrinkle, and belt to dot with change of solvents and gelator mixtures, as shown in Figure 19. Meanwhile, these organogels can self-assemble to form monomolecular or multilayer nanostructures owing to the different lengths of alkyl substituent chains. Possible assembly modes for present xerogels were proposed. The present investigation is perspective to provide new clues for the design of new nanomaterials and functional textile materials with special microstructures.

In another continuous work, the gelation behaviors of binary organogels composed of azobenzene amino derivatives and fatty acids with different alkyl chains in various organic

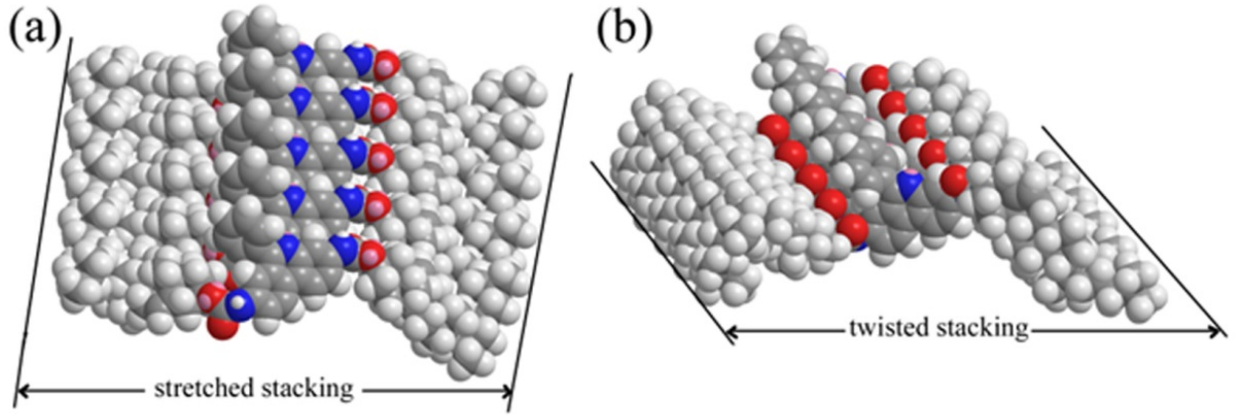


Figure 18. Rational assembly modes of CH-PY organogels in stretched stacking (a, 3.5 nm) and twisted stacking (b, 2.73 and 2.38 nm), respectively.

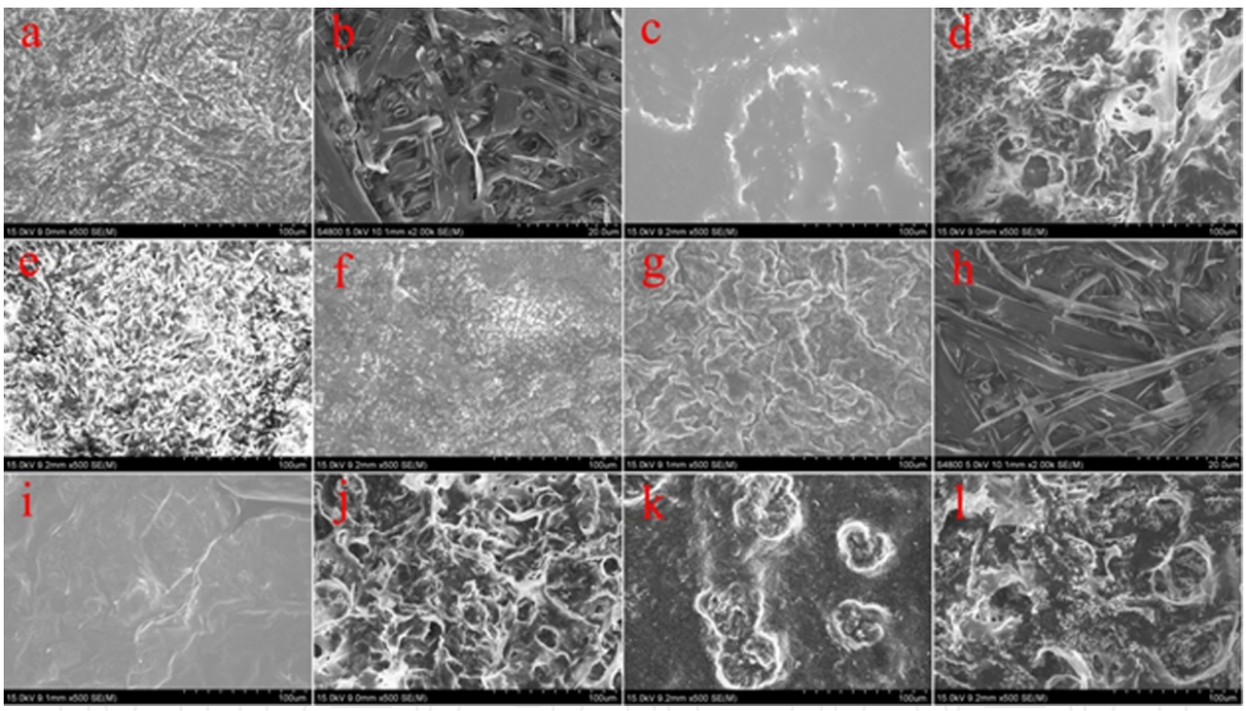


Figure 19. SEM images of xerogels. C16-Azo (a, b, c, d, e, and f) and C16-Azo-Me (g, h, i, j, k, and l) in toluene, nitrobenzene, ethanolamine, n-butyl acrylate, chloroform, and benzene, respectively.

solvents were designed and investigated [66]. The experimental results indicated that their gelation behaviors solvents can be regulated by changing the length of alkyl substituent chains and azobenzene segment. Longer alkyl chains in molecular skeletons in present gelators are favorable for the gelation of organic solvents. For the mixtures containing 4-aminoazobenzene, only C12-Azo cannot form any organogel in present solvents. While for the mixtures containing 2-aminoazotoluene, only C18-Azo-Me and C16-Azo-Me can form gel in ethanolamine, respectively. The prepared nanostructured materials have wide perspectives and many potential applications in nanoscience and material fields due to their scientific values.

http://dx.doi.org/10.5772/60796

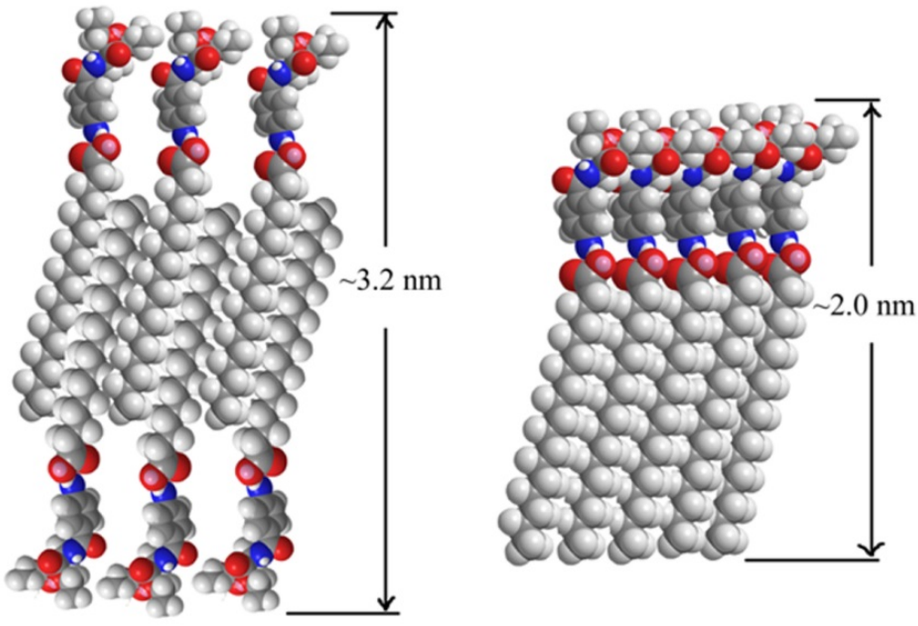


Figure 20. Two possible assembly modes for Glu-C18 organogels in different solvents.

In addition, the gelation behaviors of binary fatty acids with different length of alkyl chains and glutamic acid amino derivative in various organic solvents were designed and investigated [67]. The obtained data showed that the length of substituent chains has played an important role in the gelation properties of all gelator systems in different organic solvents. Longer alkyl chains in molecular structures in used gelator compounds are favorable for the gelation preparation of organic solvents. Considering the XRD results described and the hydrogen bonding interaction of these binary mixtures as confirmed by FT-IR measurements, two possible assembly modes of Glu-C18 were proposed and schematically shown in Figure 20. As for xerogels of Glu-C18 in different kinds of solvents (for example, toluene, isopropanol, n-butanol, and ethanolamine), the alkyl chains in neighboring molecules or stacking units will be able to penetrate easily into the empty room between the alkyl chains in another self-assembly unit. Under such self-assembly mode, the layer distance will increase to about 3.2 nm. For the xerogels of Glu-C18 in two other solvents, due to the chains parallel to the layer surface, the repeating stacking unit with length of about 2 nm was gained.

Moreover, some binary organogels based on glutamic acid derivatives and acids with different molecular skeletons were designed and prepared [68]. Their gelation behaviors in single or mixed solvents were tested as novel low molecular mass organic gelators. The experimental data showed that the solvents and molecular skeletons played a crucial role in regulating the gelation behaviors and fabrication of nanostructures. Suitable single solvents or volume ratios in ethanol/water mixed solvents seemed more favorable for the formation of supramolecular gels due to cooperation of multi-intermolecular weak forces, as shown in Figure 21. Rational assembly modes in organogels were proposed and discussed. In these gels systems, the strong π–π stacking of benzene ring and symmetrical assembly modes in molecular skeletons seemed

to have played an important role in regulating the intermolecular hydrogen bonding and orderly stacking in single/mixed solvents. In addition, the differences of gelation solvents can be mainly attributed to the variable molecular skeletons and assembly modes, which induced different types of intermolecular forces, such as π–πstacking in present cases.

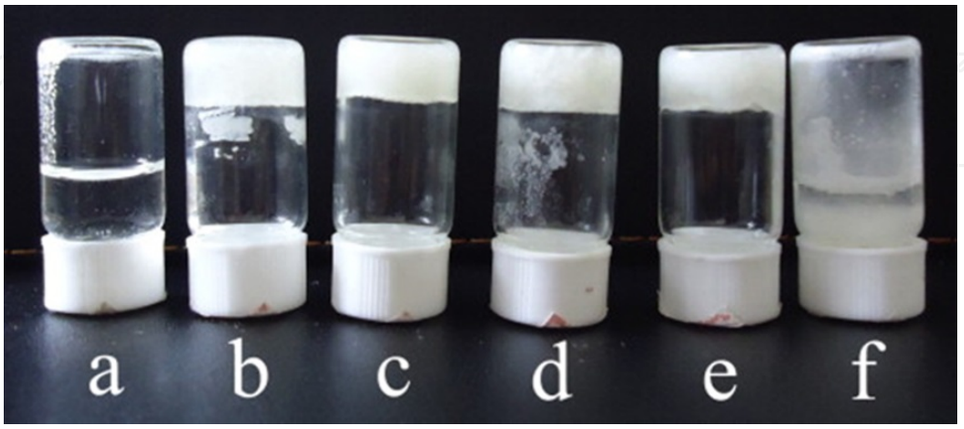


Figure 21. Photographs of GC2 organogels from ethanol/water mixed solvent with the volume ratios of 5:1, 2:1, 1:1, 1:2, 1:5, and 1:10 (a, b, c, d, e, f, respectively).

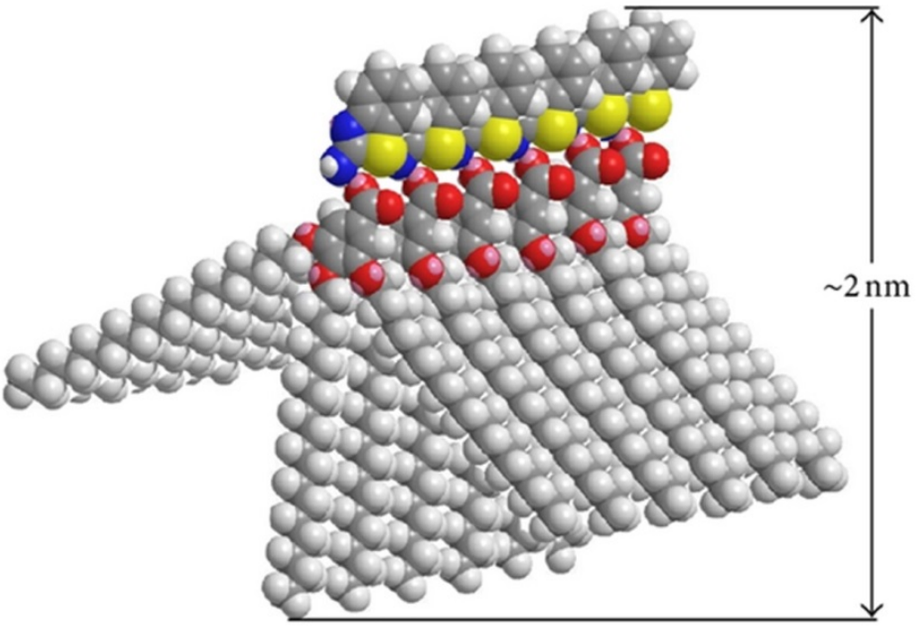


Figure 22. A reasonable self-assembly mode for S-TriC18 organogels.

In our recent study, the gelation behaviors of binary organogels composed of aminobenzimidazole/benzothiazole derivatives and benzoic acid with single/multi-alkyl substituent chain in various organic solvents were designed and investigated [69]. The experimental results

indicated that their gelation behaviors can be regulated by changing the number and length of alkyl substituent chains and benzimidazole/benzothiazole segment. The numbers of alkyl substituent chains linked to benzene rings in these acid derivatives have a profound effect upon the gelation abilities of these studied gelator mixtures. More alkyl chains in molecular skeletons in present gelators are favorable for the gelation of organic solvents. The length of alkyl substituent chains has also played an important role in changing the gelation behaviors and assembly states. Considering the obtained results and the interaction nature of the organized packing in prepared gelator system, a possible self-assembly mechanism of S-TriC18 was proposed and schematically shown in Figure 22. As for xerogels of S-TriC18, due to the S element position in benzothiazole ring, after the intermolecular hydrogen bonding and orderly stacking, the repeating unit with length of about 2 nm was obtained.

In another compared research work, some new benzimidazole/benzothiazole imide derivatives with different alkyl substituent chains were designed and synthesized. The experimental data demonstrated that the substituent alkyl chains and headgroups of benzimidazole/benzothiazole segments in gelators played an important role in the gelation properties of all derivative system in different organic solvents [70]. More alkyl chains in molecular structures in used gelator compounds are favorable for the gelation of used organic solvents. Morphological investigations indicated that the gelator molecules self-assemble into different aggregates domains from wrinkle, lamella, and belt to dot with solvent change. Spectral research suggested that there existed various H-bond between functional imide headgroups and hydrophobic force of substituent alkyl chains in molecular structures and skeletons. The present obtained results may provide new insights into preparing novel gelator systems and soft materials with special functions.

In another research system, we have investigated the preparation of organogels by self-assembly of cationic amphiphile-based GO composites [71]. Their gelation properties in different organic solvents can be changed by regulating functionalized headgroups in amphiphile compounds. Ammonium headgroup of molecular structures in the composites is more favorable for the gelation formation of different organic solvents in comparison with pyridinium headgroup. Headgroup effects of amphiphiles have been demonstrated to be an efficient means to manipulate the self-assembly of GO-based composites. Diversity of intermolecular packing between composites and solvents is presumably responsible for the presence of various nanostructures. Considering the obtained results data and the organized stacking modes in the prepared organogels, some reasonable self-assembly modes in cationic amphiphile–graphene oxide gels are proposed and schematically shown in Figure 23. As for CTAB-GO gel, due to the van der Waals force and flexibility of substituent chains in the molecular structures as well as the strong electrostatic force of ammonium headgroups with oxygen-containing functional groups at GO surface, after combination with GO, organized stacking units are gained in different solvents. As for C16Py-GO and BPy-GO nanocomposites with additional functionalized pyridinium headgroups, the π–π stacking between carbon net in GO plane and pyridine ring suggest being competitive with the electrostatic interaction and van der Waals force. So the self-assembly stacking units in nanostructures between amphiphile compounds and GO in present two systems are not organized sufficiently in comparison with

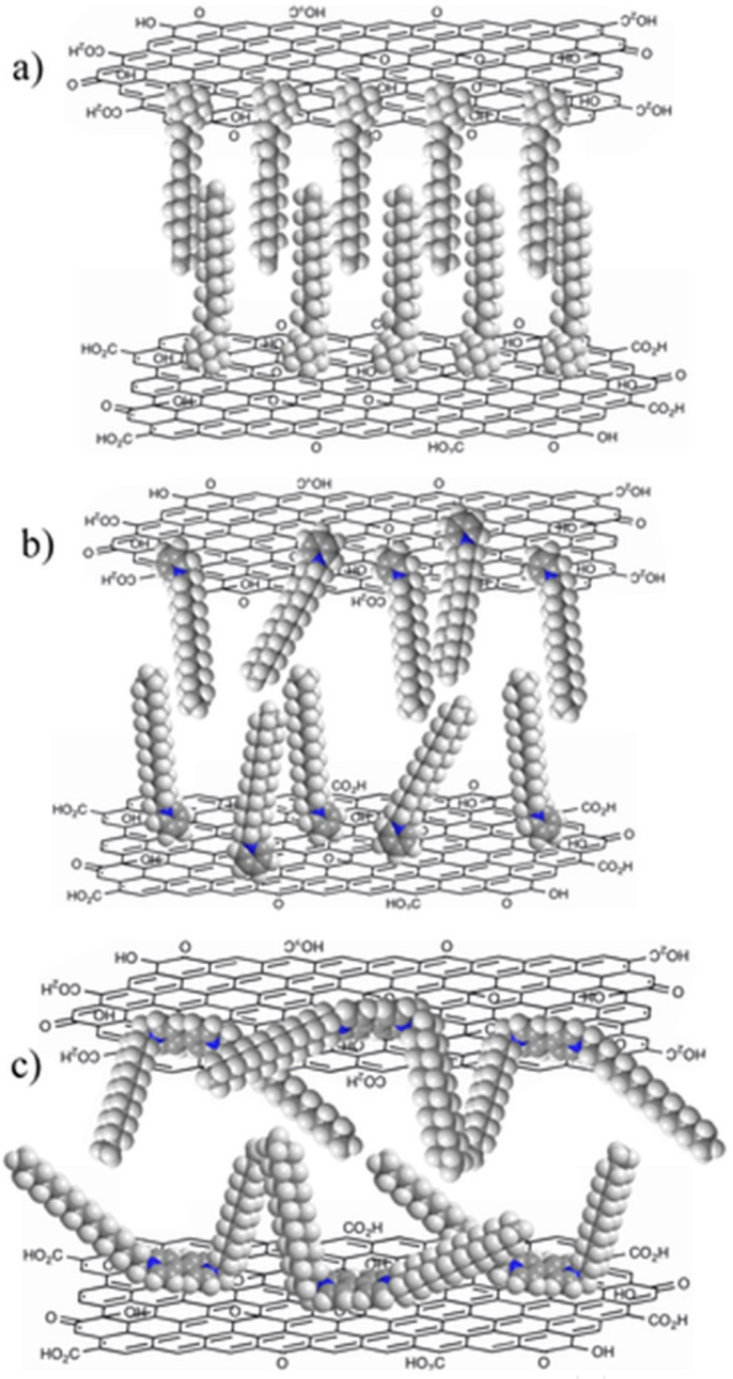


Figure 23. Scheme of different assembly modes in cationic amphiphiles–graphene oxide gels. CTAB-GO (a), C16Py-GO (b), and BPy-GO (c).

that of CTAB-GO gel due to the joint of many kinds of forces. Therefore, the present research work might renew interest and provide useful exploration in the design of self-assembled GO composites and soft matters in the future.

In addition, we have also demonstrated the formation of organogels by self-assembly of cationic gemini amphiphile–GO composites [72]. Their gelation behaviors in various organic

http://dx.doi.org/10.5772/60796

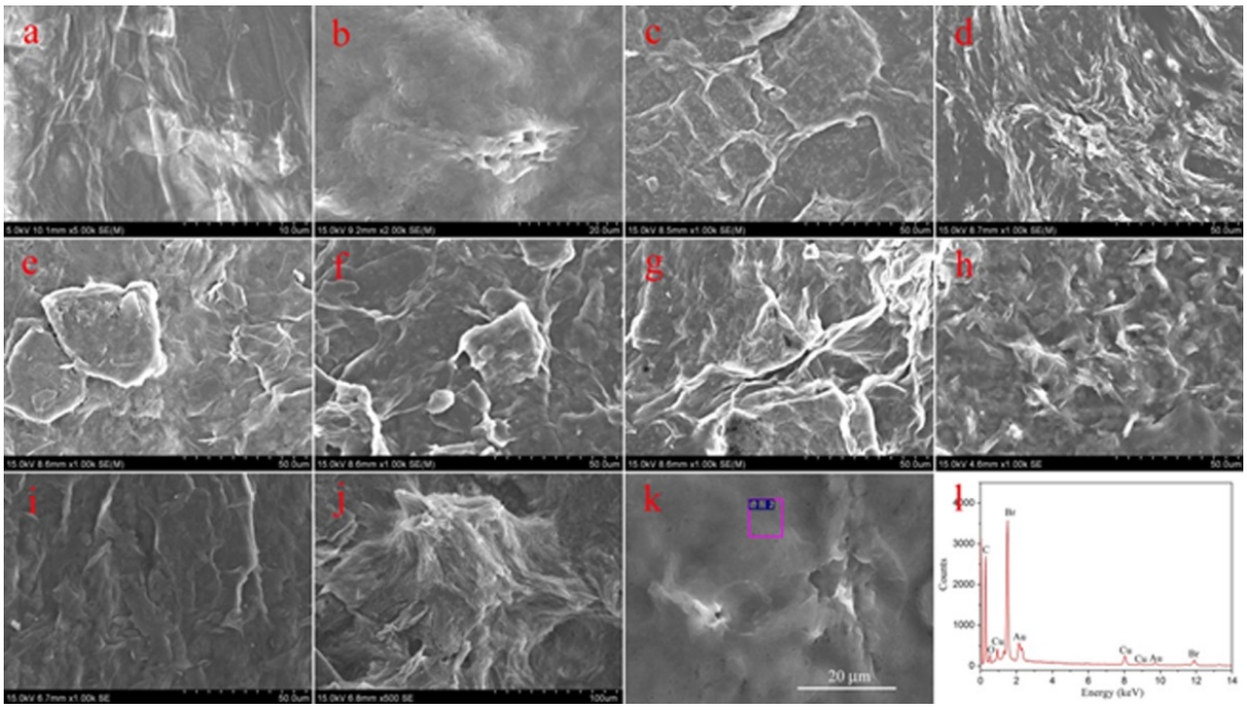


Figure 24. SEM images of xerogels. GO powder (a), C18-6-6/GO gels ((b) DMF), C18-6-12/GO gels ((c) DMF, (d) benzene, (e) toluene, (f) 1,4-dioxane, and (g) THF), and C18-6-18/GO gels ((h) cyclohexanone, (i) THF, and (j) pyridine). Typical EDXS (l) of xerogels originate from C18-6-6/GO gels in DMF (k). The Cu and Au peaks originate from the substrate of copper foil and the coated gold nanoparticles.

solvents can be regulated by changing symmetry in skeletons of amphiphiles. The substituent groups or symmetry in molecular skeletons can regulate the stacking and self-assembled nanostructures upon distinct intermolecular forces. Longer alkyl chains and symmetric structures in molecular skeletons helped to increase hydrophobic force and flexibility in self-assembly process. Diversity of intermolecular packing between composites and solvents is presumably responsible for the presence of various nanostructures, as shown in Figure 24. It is clearly investigated that the nanostructures of the as-formed xerogels of all composites in various solvents are significantly different from each other, and the morphologies and nanostructures of the self-assembled aggregates change from wrinkle and lamella to belt with the change of solvents. The difference of morphologies can be mainly attributed to the different stacking mechanisms and self-assembly modes upon interactive forces between gelators and solvent molecules. A possible mechanism for symmetry effects on self-assembly and as-prepared nanostructures is proposed. It is believed that the present amphiphile-GO self-assembled system will provide an alternative exploration for the design of new GO composite nanomaterials and soft matters.

5. Conclusion and perspectives

We are working on the design, preparation, and self-assembly of functionalized nanocomposites and nanomaterials. In this chapter, various kinds of nanocomposites including gold

nanoparticles, inorganic–organic hybrid composites, graphene oxide nanocomposites, and supramolecular gels via functionalized imide amphiphiles/binary mixtures have all been investigated and analyzed. The above work may give the potential perspective for the design and fabrication of nanomaterials and composites. In closing, new nanocomposites and nanomaterials are emerging as sensitive study platforms based on unique optical and electrical properties. In addition, supramolecular self-assembly is a key physical chemistry subject due to its close relationship to many fundamental and application scientific questions like catalysis, chirality, electron and energy transfer, single molecule science, and organic electronics. The results mentioned here only provide a cursory browse of some progress. Future research on preparation of nanocomposites and nanomaterials will depend on the less-expensive processes in order to produce low-cost nanomaterials and devices. The development in this area has been fascinating. It can be predicted that as the growth of understandings of the rules in the nanoscale, our dream to prepare functionalized nanocomposites and nanomaterials with self-assembly and organized nanostructures could be realized in future.

Acknowledgements

The authors would like to extend their thanks to the National Natural Science Foundation of China (Nos. 21473153, 21207112, and 51402253); the Natural Science Foundation of Hebei Province (No. B2013203108); the Science Foundation for the Excellent Youth Scholars from Universities and Colleges of Hebei Province (Nos. Y2011113 and YQ2013026); the Support Program for the Top Young Talents of Hebei Province; and Open Foundation of National Key Laboratory of Biochemical Engineering (Institute of Process Engineering, Chinese Academy of Sciences) for providing funds for this research.

Author details

Tifeng Jiao[1,2*], Jie Hu[1], Qingrui Zhang[1] and Yong Xiao[3]

*Address all correspondence to: tfjiao@ysu.edu.cn

1 Hebei Key Laboratory of Applied Chemistry, School of Environmental and Chemical Engineering, Yanshan University, Qinhuangdao, P. R. China

2 National Key Laboratory of Biochemical Engineering, Institute of Process Engineering, Chinese Academy of Sciences, Beijing, P. R. China

3 Qinhuangdao Environmental Protection Science Research Institute, Qinhuangdao, P. R. China

http://dx.doi.org/10.5772/60796

References

[1] Vashist SK, Luong JHT. Recent advances in electrochemical biosensing schemes using graphene and graphene-based nanocomposites. Carbon 2015;84:519–50.

[2] Hu K, Kulkarni DD, Choi I, Tsukruk VV. Graphene-polymer nanocomposites for structural and functional applications. Prog Polymer Sci 2014;39(11):1934–72.

[3] Mutiso RM, Winey KI. Electrical properties of polymer nanocomposites containing rod-like nanofillers. Prog Polymer Sci 2015;40:63–84.

[4] Zhu S, Segura T. Hydrogel-based nanocomposites of therapeutic proteins for tissue repair. Curr Opin Chem Eng 2014;4:128–36.

[5] Campbell TA, Ivanova OS. 3D printing of multifunctional nanocomposites. Nano Today 2013;8(2):119–20.

[6] Lee YS. Self-Assembly and Nanotechnology Systems: Design, Characterization, and Applications. New Jersey: John Wiley & Sons, Inc.; 2011.

[7] Pelesko JA. Self Assembly: The Science of Things That Put Themselves Together. London: Chapman and Hall/CRC Press; 2007.

[8] Jiao T, Wang S, Zhou J. Molecular design and supramolecular assemblies of novel amphiphiles with special molecular structures in organized molecular films. In: Rahman M. (ed.) Nanomaterials. Rijeka: InTech; 2011, pp.315–46.

[9] Ghosh SK, Pal T. Interparticle coupling effect on the surface plasmon resonance of gold nanoparticles: from theory to applications. Chem Rev 2007;107:4797–862.

[10] Katz E, Willner I. Integrated nanoparticle-biomolecule hybrid systems: synthesis, properties, and applications. Angewandte Chemie International Edition 2004;43(45): 6042–108.

[11] Daniel MC, Astruc D. Gold nanoparticles: assembly, supramolecular chemistry, quantum-size-related properties, and applications toward biology, catalysis, and nanotechnology. Chem Rev 2004;104:293–346.

[12] Liao J, Bernard L, Langer M, Schoenberger C, Calame M. Reversible formation of molecular junctions in 2D nanoparticle arrays. Adv Mater 2006;18(18):2444–7.

[13] Klajn R, Bishop KJM, Grzybowski BA. Light-controlled self-assembly of reversible and irreversible nanoparticle suprastructures. Proc Nat Acad Sci USA 2007;104:10305–9.

[14] Koplin E, Niemeyer CM, Simon U. Formation of electrically conducting DNA-assembled gold nanoparticle monolayers. J Mater Chem 2006;16:1338–44.

[15] Meister A, Drescher S, Mey I, Wahab M, Graf G, Garamus VM, Hause G, Mo1gel HJ, Janshoff A, Dobner B, Blume A. Helical nanofibers of self-assembled bipolar phospholipids as template for gold nanoparticles. J Phys Chem B 2008;112:4506–11.

[16] Jadzinsky PD, Calero G, Ackerson CJ, Bushnell DA, Kornberg RD. Structure of a thiol monolayer-protected gold nanoparticle at 1.1 Å resolution. Science 2007;318:430–3.

[17] Wen Y, Jiang X, Yin G, Yin J. Multi-responsive amphiphilic gold nanoparticles (AuNPs) protected by poly(ether amine) (PEA). Chem Commun 2009;43:6595–7.

[18] Song WJ, Du JZ, Sun TM, Zhang PZ, Wang J. Gold nanoparticles capped with polyethyleneimine for enhanced siRNA delivery. Small 2010;6:239–46.

[19] Ko S, Park TJ, Kim HS, Kim JH, Cho YJ. Directed self-assembly of gold binding polypeptide-protein: a fusion proteins for development of gold nanoparticle-based SPR immunosensors. Biosens Bioelectron 2009;24:2592–7.

[20] George J, Thomas KG. Surface plasmon coupled circular dichroism of Au nanoparticles on peptide nanotubes. J Am Chem Soc 2010;132:2502–3.

[21] Cho EC, Au L, Zhang Q, Xia Y. The effects of size, shape, and surface functional group of gold nanostructures on their adsorption and internalization by cells. Small 2010;6:517–22.

[22] Jiao T, Wang Y, Guo W, Zhang Q, Yan X, Chen J, Wang L, Xie D, Gao F. Synthesis and photocatalytic property of gold nanoparticles by using a series of bolaform Schiff base amphiphiles. Mater Res Bull 2012;47(12):4203–9.

[23] Jiao T, Wang Y, Zhang Q, Yan X, Chen J, Zhou J, Gao F. Preparation and photocatalytic property of gold nanoparticles by using two bolaform cholesteryl imide derivatives. J Dispers Sci Technol 2013;34(12):1675–82.

[24] Huang H, Sun G, Hu J, Jiao T. Single-step synthesis of $LaMnO_3$/MWCNT nanocomposites and their photocatalytic activities. Nanomater Nanotechnol 2014;4:27.

[25] Wang S, Lv F, Jiao T, Ao J, Zhang X, Jin F. A novel porous carrier found in nature for nanocomposite materials preparation: a case study of Artemia Egg shell-supported TiO_2 for formaldehyde removal. J Nanomater 2014;2014:963012.

[26] Zhang Q, Du Q, Hua M, Jiao T, Gao F, Pan B. Sorption enhancement of lead ions from water by surface charged polystyrene-supported nano-zirconium oxide composites. Environ Sci Technol 2013;47(12):6536–44.

[27] Zhang Q, Du Q, Jiao T, Pan B, Zhang Z, Sun Q, Wang S, Wang T, Gao F. Selective removal of phosphate in waters using a novel of cation adsorbent: Zirconium phosphate (ZrP) behavior and mechanism. Chem Eng J 2013;221:315–21.

[28] Zhang Q, Du Q, Jiao T, Zhang Z, Wang S, Sun Q, Gao F. Rationally designed porous polystyrene encapsulated zirconium phosphate nanocomposite for highly efficient fluoride uptake in waters. Scientific Rep 2013;3:2551.

[29] Xing R, Jiao T, Feng L, Zhang Q, Zou Q, Yan X, Zhou J, Gao F. Photothermally-induced molecular self-assembly of macroscopic peptide-inorganic hybrid films. Sci Adv Mater 2015;7:in press.

[30] Liang D, Cui C, Hu H, Wang Y, Xu S, Ying B, Li P, Lu B, Shen H. One-step hydrothermal synthesis of anatase TiO_2/reduced graphene oxide nanocomposites with enhanced photocatalytic activity. J Alloys Compd 2014;582:236–40.

[31] Ullah K, Zhu L, Meng ZD, Ye S, Sun Q, Oh WC. A facile and fast synthesis of novel composite Pt-graphene/TiO_2 with enhanced photocatalytic activity under UV/Visible light. Chem Eng J 2013;231:76–83.

[32] Bai XJ, Wang L, Zhu YF. Visible photocatalytic activity enhancement of $ZnWO_4$ by graphene hybridization. ACS Catal 2012;2:2769–78.

[33] Sun L, Shao R, Tang LQ, Chen ZD. Synthesis of $ZnFe_2O_4$/ZnO nanocomposites immobilized on graphene with enhanced photocatalytic activity under solar light irradiation. J Alloys Compd 2013;564:55–62.

[34] Xu JJ, Ao YH, Chen MD. A simple method for the preparation of Bi_2WO_6-reduced graphene oxide with enhanced photocatalytic activity under visible light irradiation. Mater Lett 2013;92:126–8.

[35] Li T, Shen JF, Li N, Ye MX. Hydrothermal preparation, characterization and enhanced properties of reduced graphene-$BiFeO_3$ nanocomposite. Mater Lett 2013;91:42–4.

[36] Lv T, Pan LK, Liu XJ, Lu T, Zhu G, Sun Z. Enhanced photocatalytic degradation of methylene blue by ZnO-reduced graphene oxide composite synthesized via microwave-assisted reaction. J Alloys Compd 2011;509:10086–91.

[37] Jiang LX, Li KX, Yan LS, Dai YH, Huang ZM. Preparation of Ag(Au)/graphene-TiO_2 composite photocatalysts and their catalytic performance under simulated sunlight irradiation. Chinese J Catal 2012;33(12):1974–81.

[38] Zhang DF, Pu XP, Ding GQ, Shao X, Gao YY, Liu JX, Gao MC, Li Y. Two-phase hydrothermal synthesis of TiO_2-graphene hybrids with improved photocatalytic activity. J Alloys Compd 2013;572:199–204.

[39] Hu J, Ma J, Wang L, Huang H. Synthesis and photocatalytic properties of $LaMnO_3$-graphene nanocomposites. J Alloys Compd 2014;583:539–45.

[40] Hu J, Ma J, Wang L, Huang H. Preparation of $La_{1-x}Sr_xMnO_3$ /graphene thin films and their photocatalytic activity. Mater Sci Eng B 2014;180:46–53.

[41] Hu J, Ma J, Wang L, Huang H, Ma L. Preparation, characterization and photocatalytic activity of Co-doped $LaMnO_3$/graphene composites, Powder Technol 2014;254:556–62.

[42] Hu J, Wang L, Ma J, Huang H. Study on the preparation and photocatalytic performance of the $LaNiO_3$/graphene composite film. Rare Metal Mater Eng 2014;43(7):1736–41.

[43] Hu J, Wang L, Shi L, Huang H. Preparation of $La_{1-x}Ca_xMnO_3$ perovskite-graphene composites as oxygen reduction reaction electrocatalyst in alkaline medium. J Power Sources 2014;269:144–51.

[44] Hu J, Men J, Ma J, Huang H. Preparation of $LaMnO_3$/graphene thin films and their photocatalytic activity. J Rare Earths 2014;32(12):1127–35.

[45] Basrur VR, Guo J, Wang C, Raghavan SR. Synergistic gelation of silica nanoparticles and a sorbitol-based molecular gelator to yield highly-conductive free-standing gel electrolytes. ACS Appl Mater Interfaces 2013;5:262–7.

[46] van der Laan S, Feringa BL, Kellogg RM, van Esch J. Remarkable polymorphism in gels of new azobenzene bis-urea gelators. Langmuir 2002;18:7136–40.

[47] Oh H, Jung BM, Lee HP, Chang JY. Dispersion of single walled carbon nanotubes in organogels by incorporation into organogel fibers. J Colloid Interface Sci 2010;352:121–7.

[48] Delbecq F, Tsujimoto K, Ogue Y, Endo H, Kawai T. N-stearoyl amino acid derivatives: potent biomimetic hydro/organogelators as templates for preparation of gold nanoparticles. J Colloid Interface Sci 2013;390:17–24.

[49] George SJ, Ajayaghosh A. Self-assembled nanotapes of oligo (p-phenylene vinylene)s: sol-gel-controlled optical properties in fluorescent π-electronic gels. Chemistry-A European Journal 2005; 11: 3217-3227.

[50] Kuroiwa K, Shibata T, Takada A, Nemoto N, Kimizuka N. Heat-set gel-like networks of lipophilic Co(II) triazole complexes in organic media and their thermochromic structural transitions. Journal of the American Chemical Society 2004; 126: 2016-2021.

[51] Ajayaghosh A, Chithra P, Varghese R. Self-assembly of tripodal squaraines: cation-assisted expression of molecular chirality and change from spherical to helical morphology. Angewandte Chemie International Edition 2007; 46: 230-233.

[52] Xin F, Zhang H, Hao B, Sun T, Kong L, Li Y, Hou Y, Li S, Zhang Y, Hao A. Controllable transformation from sensitive and reversible heat-set organogel to stable gel induced by sodium acetate. Colloids and Surfaces A: Physicochem Eng Aspects 2012;410:18–22.

[53] Iwanaga K, Sumizawa T, Miyazaki M, Kakemi M. Characterization of organogel as a novel oral controlled release formulation for lipophilic compounds. Int J Pharmaceut 2010;388:123–8.

[54] Lofman M, Koivukorpi J, Noponen V, Salo H, Sievanen E. Bile acid alkylamide derivatives as low molecular weight organogelators: systematic gelation studies and qualitative structural analysis of the systems. J Colloid Interface Sci 2011;360:633–44.

[55] Bastiat G, Plourde F, Motulsky A, Furtos A, Dumont Y, Quirion R, Fuhrmann G, Leroux JC. Tyrosine-based rivastigmine-loaded organogels in the treatment of Alzheimer's disease. Biomaterials 2010;31:6031–8.

[56] Tao ZG, Zhao X, Jiang XK, Li ZT. A hexaazatriphenylene-based organogel that responds to silver(I) with high selectivity under aqueous condition. Tetrahedron Lett 2012;53:1840–2.

[57] Miyamoto K, Jintoku H, Sawada T, Takafuji M, Sagawa T, Ihara H. Informative secondary chiroptics in binary molecular organogel systems for donor-acceptor energy transfer. Tetrahedron Lett 2011;52:4030–5.

[58] Jiao T, Wang Y, Gao FQ, Zhou J, Gao FM. Photoresponsive organogel and organized nanostructures of cholesterol imide derivatives with azobenzene substituent groups. Prog Nat Sci: Mater Int 2012;22(1):64–70.

[59] Jiao T, Gao FQ, Wang Y, Zhou J, Gao FM, Luo X. Supramolecular gel and nanostructures of bolaform and trigonal cholesteryl derivatives with different aromatic spacers. Curr Nanosci 2012;8(1):111–6.

[60] Jiao T, Wang R, Zhang Q, Yan X, Zhou J, Gao F. Nanostructures and substituent alkyl chains effect on assembly of organogels based on some glutamic acid diethyl ester imide derivatives. Curr Nanosci 2013;9(4):536–42.

[61] Jiao T, Wang Y, Zhang Q, Zhou J, Gao F. Regulation of substituent groups on morphologies and self-assembly of organogels based on some azobenzene imide derivatives. Nanoscale Res Lett 2013;8:160.

[62] Jiao T, Huang Q, Zhang Q, Xiao D, Zhou J, Gao F. Self-assembly of organogels via new luminol imide derivatives: diverse nanostructures and substituent chain effect. Nanoscale Res Lett 2013;8:278.

[63] Jiao T, Gao F, Zhang Q, Zhou J, Gao F. Spacer effect on nanostructures and self-assembly in organogels via some bolaform cholesteryl imide derivatives with different spacers. Nanoscale Res Lett 2013;8:406.

[64] Jiao TF, Gao FQ, Shen XH, Zhang QR, Zhang XF, Zhou JX, Gao FM. Self-assembly and nanostructures in organogels based on a bolaform cholesteryl imide compound with conjugated aromatic spacer. Materials 2013;6(12):5893–906.

[65] Hu Y, Li Q, Hong W, Jiao T, Xing G, Jiang Q. Characterization of binary organogels based on some azobenzene compounds and alkyloxybenzoic acids with different chain lengths. J Spectrosc 2014;2014:970827.

[66] Guo H, Jiao T, Shen X, Zhang Q, Li A, Gao F. Preparation and characterization of binary organogels via some azobenzene amino derivatives and different fatty acids: self-assembly and nanostructures. J Spectrosc 2014;2014:758765.

[67] Jiao T, Xing R, Shen X, Zhang Q, Zhou J, Gao F. Investigation of orderly nanostructures and assembly modes of binary organogels via glutamic acid amino derivative and different fatty acids. Integr Ferroelect: Int J 2014;151(1):31–41.

[68] Guo H, Jiao T, Shen X, Zhang Q, Li A, Zhou J, Gao F. Binary organogels based on glutamic acid derivatives and different acids: solvent effect and molecular skeletons on self-assembly and nanostructures. Colloids Surfaces A: Physicochem Eng Aspects 2014;447:88–96.

[69] Jiao T, Ma K, Shen X, Zhang Q, Li X, Zhou J, Gao F. Self-assembly and soft material preparation of binary organogels via aminobenzimidazole/benzothiazole and acids with different alkyl substituent chains. J Nanomater 2013;2013:762732.

[70] Shen X, Jiao T, Zhang Q, Guo H, Lv Y, Zhou J, Gao F. Nanostructures and self-assembly of organogels via benzimidazole/benzothiazole imide derivatives with different alkyl substituent chains. J Nanomater 2013;2013:409087.

[71] Jiao T, Wang Y, Zhang Q, Yan X, Zhao X, Zhou J, Gao F. Self-assembly and headgroup effect in nanostructured organogels via cationic amphiphile-graphene oxide composites. PLoS ONE 2014;9(7):e101620.

[72] Jiao T, Wang Y, Zhang Q, Yan X, Zhao X, Huo Q, Zhou J, Gao F. Organogels via gemini amphiphile-graphene oxide composites: self-assembly and symmetry effect. Sci Adv Mater 2015;7:in press.

IntechOpen